Manuscript prepared for Atmos. Chem. Phys.
with version 5.0 of the LaTeX class copernicus.cls.
Date: 23 May 2014

Systematic analysis of tropospheric NO_2 long-range transport events detected in GOME-2 satellite data

A. W. Zien[1], A. Richter[1], A. Hilboll[1], A.-M. Blechschmidt[1], and J. P. Burrows[1]

[1]Institute for Environmental Physics, University of Bremen

Correspondence to: A. W. Zien (achim@zien.me)

Abstract. Intercontinental long-range transport (LRT) events of NO_2 relocate the effects of air pollution from emission regions to remote, pristine regions. We detect transported plumes in tropospheric NO_2 columns measured by the GOME-2 / MetOp-A instrument with a specialized algorithm and trace the plumes to their sources using the HYSPLIT lagrangian transport model. With this algorithm we find 3808 LRT events over the ocean for the period 2007 to 2011. LRT events occur frequently in the mid-latitudes, emerging usually from coastal high-emission regions. In the free troposphere, plumes of NO_2 can travel for several days to the polar oceanic atmosphere or to other continents. They travel along characteristic routes and originate from both continuous anthropogenic emission and emission events such as bush fires. Most NO_2 LRT events occur during autumn and winter months, when meteorological conditions and emissions are most favorable. The evaluation of meteorological data shows that the observed NO_2 LRT is often linked to cyclones passing over an emission region.

1 Introduction

The transport of atmospheric pollution over long distances mostly affects long-lived species, such as CO, SO_2 and O_3. During long-range transport (LRT) of chemical species, trace gases are transported over intercontinental distances, relocating gases from emission to remote and pristine regions. As a result, air pollution has to be regarded as a global instead of a local phenomenon. Under certain conditions, this can also affect short-lived species which are commonly considered to be bounded to their emission regions.

While long-lived gas species can also mix slowly in the atmosphere to reach remote regions, a short-lived species has to travel fast before it is eventually converted into other species.

Here, we investigate the long-range transport of NO_2. Its lifetime in the planetary boundary layer (PBL) amounts to a few hours, depending on the strength of solar irradiation and on the available radical species. This, combined with low wind speeds near the surface, makes long-range transport of anthropogenic NO_2 in the planetary boundary layer very unlikely.

Still, satellite observations of NO_2 frequently exhibit such long-range transport events and allow a systematic analysis of their properties – such as their NO_2 content, altitude and age.

NO_2 is a toxic trace gas which can harm respiratory organs. A major fraction of the emissions takes place in the form of NO which then rapidly converts to NO_2 until the Leighton photostationary state is achieved at a ratio of $NO/NO_x \approx 0.2$–0.8 (Ehhalt et al., 1992) – depending on radiative flux, available radical species and air pressure. NO_x is defined as the sum of the species NO and NO_2.

NO and NO_2 emissions originate from various sources. The dominant sources are anthropogenic emissions from combustion processes in transportation, power plants, industry and agricultural biomass burning, as well as natural sources such as lightning emissions, natural biomass burning and microbial soil emissions. Martin et al. (2003) report a total yearly NO_x emission rate of $43\,TgN/a$ in 1996–1997, with anthropogenic sources contributing roughly half of the emissions.

NO_2 also reacts with OH to form HNO_3 which permanently removes the NO_2 from the air masses and results in acid rain. This is the major atmospheric loss of NO_2. Besides that, NO_2 directly impacts the ozone cycle in the troposphere, where it favors O_3 production. The presence of OH and volatile organic compounds (VOCs) can amplify this effect leading to the well known photochemical ozone smog. As the lifetime of NO_2 is relatively short, ozone smog formation is usually limited to polluted regions. However, in air

masses containing large amounts of biogenic VOCs, addition of NO_x from lightning, biomass burning or potentially from long-range transport can also lead to ozone production. At very large NO_2 concentrations, ozone formation is suppressed leading to lower ozone values in pollution hotspots.

The lifetime of NO_2 ranges from around 8 hours in a typical planetary boundary layer scenario to a few days in the upper troposphere (Ehhalt et al., 1992; Beirle et al., 2011).

A long-range transport (LRT) event denotes a distinct plume of trace gas being exported from an emission region to a downwind region over a long distance, typically several thousand kilometers. While long-range transport could, in principle, take place in the boundary layer, it is more likely that the actual transport happens after convection out of the planetary boundary layer into the free troposphere, where wind speeds are much higher, due to a lack of interaction with the surface.

For NO_2, long-range transport will predominantly take place in the free troposphere, where – in addition to the higher windspeed – its lifetime is extended to up to four days, due to lower concentrations of radical species. As NO_2 is mainly emitted in the boundary layer, this phenomenon could be expected to be rare. For its occurrence, there has to be a mechanism to lift polluted air-masses into the free troposphere.

Once this happens, the NO_2 is transported from emission regions to remote, pristine regions, e.g. over the oceans, into polar regions or to other continents. This means that the NO_2 in these cases does not only affect its source region, but has regional or even global impacts.

As this study will show, NO_2 long-range transport plumes can have a horizontal extent of more than $1000\,\mathrm{km}$. Due to this large extent, plumes are subject to horizontal shear winds. This results in filamentation and typical arc-like structures after a few days. The plume will also disperse over the course of the transport, typically after a few days (Rastigejev et al., 2010).

Due to chemical conversion, physical dispersion and filamentation, intercontinental NO_2 long-range transport events are usually seen departing from an emission region to the ocean, but they dissolve before arriving on another continent. Once lifted, the ratio of NO/NO_x will change leading to a reduction of NO_2 and a larger, unobserved reservoir of NO.Over the course of transport, NO_2 partly is converted into peroxyacyl nitrate (PAN) and other reservoir species, which may then release NO_2 upon descent, when concentrations of radical species, pressure and temperature increase (Singh and Hanst, 1981; Schultz et al., 1998; Walker et al., 2010). Both processes, direct long-range transport of NO_x and transport of its reservoir species lead to an effective relocation of NO_x emissions.

NO_2 concentrations can be observed both via in-situ and remote sensing methods. As long-range transport is a large-scale phenomenon, we use data from satellite remote sensing observations for our large-scale and global analysis.

However, NO_2 long-range transport events are rarely seen in most satellite data products. This can lead to the false assumption that they also occur rarely. The reason for this lies in the common practice of filtering cloudy pixels from satellite observations. This is done because clouds complicate the radiative transfer and make the retrieval of trace gas concentrations harder. In particular, the sensitivity to NO_2 in the boundary layer is reduced in presence of clouds for most common observation scenarios.

If we omit the cloud filter, we observe many long-range transport events just by browsing through the data. Due to their intermitting occurrence and rapid movement, such events are best seen in daily or orbit-wise data – not in data averaged over longer time periods.

For different chemical species, long-range transport events have received more attention in the last few years. The Hemispheric Transport of Air Pollutants (HTAP) task force was created to collect data and knowledge on this phenomenon and assess its impact on the environment. In their report (Dentener et al., 2010), they find that a significant fraction of ozone pollution in the Northern Hemisphere is driven by transport from remote sources, mostly of ozone precursors such as methane and NO_x. They expect the resulting increased base levels of ozone to lead to an increased threat to human health and crop yields.

There are a number of satellite based case studies of individual events of NO_2 long-range transport. Wenig et al. (2003) report the first observation of such an event, a plume emitted from South Africa in May 1998. In their study, a high-pressure system favored a localized build-up of NO_2 concentrations which were then rapidly lifted to an altitude of $2-6\,\mathrm{km}$ above mean sea level (a.m.s.l.) by a passing low-pressure system. There, longer lifetime and higher wind speeds allowed the NO_2 to travel onto the open ocean.

Stohl et al. (2003) investigated an episode in which an explosively developing cyclone transported a significant plume of NO_2 over the Atlantic in about one day. The NO_2 was lifted upwards by a warm conveyor belt (WCB). In a climatological study, they find intercontinental express highways between North America and Europe which are much stronger in winter and can contribute about 2–$3\,\mathrm{pptv}$ of European NO_2 concentrations during winter.

Schaub et al. (2005) discuss an event during which NO_2 from the central German Ruhr area was lifted into the free troposphere (over the course of a day) and transported into the Alps where a significant increase in concentrations was measured in-situ on the Zugspitze and on multiple sites in Switzerland.

Studies by Spichtinger et al. (2001) and Riuttanen et al. (2013) illustrate further aspects of individual, observed transport events.

Unfortunately, there are – to our knowledge – no in-situ measurements of tropospheric NO_2 long-range transports by aircraft which would allow us to determine typical vertical

concentration profiles and verify the results of this study with non-satellite observations.

Lin et al. (2010) have focussed on modeling NO_2 long-range transport with global chemical transport models (GCTMs). They find that $8-15\,\%$ of NO_x emissions are transported over $1000\,km$ from their source regions, using WRF-Chem and CMAQ for rapid vertical transport and MOZART as GCTM. They also note that in most GCTMs, rapid convection (such as in frontal passages) is not adequately represented, which biases the simulation of long-range transport events. The modeling of horizontal transport tends to dilute the plumes' boundaries, which are found to be rather sharp in observational data.

So far there has – to our knowledge – not been a systematic study of NO_2 long-range transport events using observational data. Such studies are necessary in order to judge the impact of NO_2 long-range transport on the atmospheric chemistry in pristine and sensitive environments such as the Arctic and to validate its impact as estimated from GCTMs.

In this study, we have used daily maps of tropospheric NO_2 from the GOME-2 / MetOp-A instrument (Sect. 2). We implemented an algorithm to detect long-range transport events over the ocean in this timeseries of two-dimensional data (Sect. 3). This allows us to perform a systematic study of long-range transport of NO_2. We retrieved additional properties of the detected plumes with backtrajectories from the HYSPLIT lagrangian transport model. We determined the most likely backtrajectory using a scoring system and validated the plume to be a long-range transport event. We further describe the limitations of this study (Sect. 4). After obtaining this dataset, we have performed four case studies on remarkable and typical long-range transports (Sect. 5). We examined statistical properties of the obtained dataset and investigated typical meteorological conditions accompanying the emission of NO_2 long-range transport plumes (Sect. 6).

2 GOME-2 satellite observations

This study uses data from the GOME-2 / MetOp-A satellite instrument, which is converted to daily 2-D tropospheric NO_2 vertical column density maps for further analysis.

GOME-2 (Callies et al., 2000) are a series of instruments aboard the MetOp satellites which measure trace gas optical depths via differential optical absorption spectroscopy of scattered sunlight (DOAS; Solomon et al., 1987; Platt and Stutz, 2007). The first GOME-2 instrument started operation on 4 January 2007 aboard MetOp-A and provides continuous observations until now. GOME-2 is an improved version of GOME (Burrows et al., 1999) and SCIAMACHY (Burrows et al., 1995; Bovensmann et al., 1999).

MetOp-A is on a sun-synchronous orbit at an altitude of $800\,km$ a.m.s.l., giving measurements at roughly the same local time for all sub-polar latitudes. It orbits the Earth 14 times a day on a near-polar orbit and has an equator crossing time of 09:30 local time in descending node. GOME-2 measures in a sweeping-broom configuration, with a pixel size of $80 \times 40\,km^2$. The swath width of $1960\,km$ yields a nearly global coverage every day.

For the DOAS analysis, the optical depth is derived from nadir observations $I_{nadir}(\lambda)$ and daily solar irradiance measurements $I_0(\lambda)$. Absorption features of trace gases (and other effects like the Ring-spectrum) are fitted in a suitable wavelength window. The low-variance part is approximated by a polynomial function. The remaining high-variance parts of the measured optical depth are fitted by reference spectra (from laboratory measurements) for the relevant trace gases in this regime. Given the absorption coefficient and employing the Beer-Lambert law, this yields the trace gas density integrated along the light path for the selected species. More details on the DOAS analysis can be found in Richter et al. (2011) and references therein.

For this study, we use data from the Bremen GOME-2 slant column density product as described by Richter and Burrows (2002) and Richter et al. (2011), which includes an NO_2 fit in the wavelength range from 425–$497\,nm$. We analyze data from 4 January 2007 to 31 December 2011. In order to improve spatial resolution and to reduce the effects of photochemistry on NO_2, backscan-pixels, ascending node pixels and pixels with a solar zenith angle of $sza > 80°$ were excluded from the data.

In most previous work, our GOME-2 NO_2 product uses FRESCO+ (Wang et al., 2008) to determine the cloud fraction and excludes pixels with a cloud fraction of $CF \geq 0.2$. However, for the analysis of NO_2 long-range transport, no cloud-filtering was applied to the data. A systematic study of this phenomenon requires us to include cloudy data in the study, as many transport events are associated with frontal systems which are accompanied by clouds and these events would otherwise only be partly visible or entirely missing in the data.

In this study, we are interested in the tropospheric NO_2 distribution only, so we apply a stratospheric correction, removing any stratospheric contributions. Here, the stratospheric part of the measured NO_2 column is estimated from a 3-D chemical transport model (CTM), the B3dCTM (Aschmann et al., 2009; Hilboll et al., 2013). The obtained stratospheric NO_2 is offset to represent the zonally averaged NO_2 in the reference sector (Richter and Burrows, 2002): a strip over the remote Pacific – between $180°W$ and $140°W$ – which is assumed to not contain any tropospheric NO_2. This is then converted to a stratospheric slant column density map (via a stratospheric air-mass factor, see below) and subsequently subtracted from the total slant column density map to produce the tropospheric slant column density map.

This value contains no information about the altitude of the measured trace gas. To estimate the NO_2 pollution in a pixel, we need to model the lightpath and apply a corresponding correction – called the air-mass factor (AMF) – to obtain the vertical column density.

$$\mathrm{VCD} = \frac{\mathrm{SCD}}{\mathrm{AMF}} \quad (1)$$

The air-mass factor for a scene is derived from radiative transfer models initialized with a suitable scenario.

As typical NO_2 long-range transport events extend over hundreds of kilometers, we grid the retrieved data onto a grid with a cell size of $0.5° \times 0.5°$ – to speed up computing times and reduce retrieval uncertainties – without significantly impacting our results.

2.1 Vertical column densities (VCDs) in partially cloudy scenes

To convert the NO_2 slant-column densities into vertical-column densities, we need to determine the air-mass factor, which interrelates these two. The air-mass factor describes, by which factor the vertical column density differs from the slant column density due to the radiative transfer (RT) from light source to observer.

We refrain from using a cloud-filter which removes satellite observations that show a certain degree of cloudiness. Long-range transport events are commonly linked to frontal systems and thus to cloud formation. In order to observe these events, we need to take cloudy pixels into account (see Fig. 1).

For the computation of air-mass factor, we use the SCIATRAN 3.1 radiative transfer model (Rozanov et al., 2005; Rozanov et al.) to calculate altitude dependent block air-mass factors (BAMF). The block air-mass factor denotes the sensitivity of the observations to a trace gas at a given altitude (Palmer et al., 2001). It can be visualized as the mean factor of light-path enhancement at a specific altitude. Neglecting saturation effects, the block air-mass factor relates to the air-mass factor as:

$$\mathrm{AMF} = \frac{\int_{\mathrm{surface}}^{\mathrm{ToA}} \mathrm{BAMF(h)}\rho(\mathrm{h})\mathrm{dh}}{\int_{\mathrm{surface}}^{\mathrm{ToA}} \rho(\mathrm{h})\mathrm{dh}} \quad (2)$$

Clouds alter the block air-mass factor in multiple ways. The exact behavior depends on geometry and cloud properties. Typical effects are (Hild et al., 2002; Boersma et al., 2004; Beirle et al., 2009):

- The cloud provides a surface of high reflectivity. The block air-mass factor is enhanced close over the cloud top (albedo effect).
- Inside the cloud, multiple scattering takes place which elongates the mean light path and leads to a further increased block air-mass factor in the top layers. Less light penetrates into the lower layers, which in turn rapidly decreases the block air-mass factor towards the cloud bottom (multiple scattering effect).

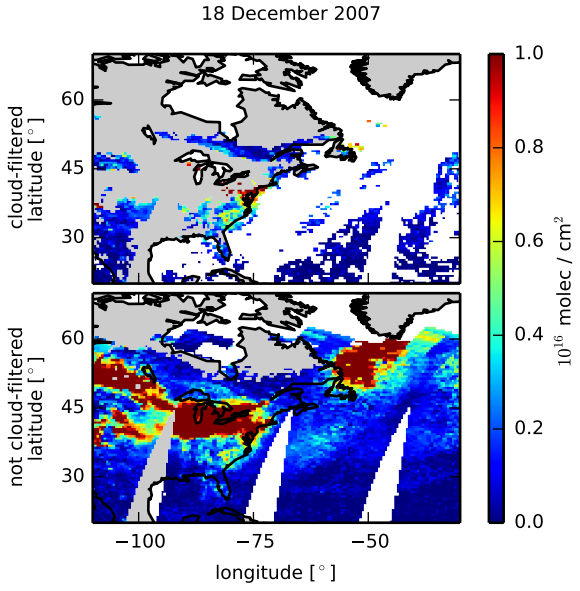

Fig. 1. GOME-2 tropospheric NO_2 vertical column density with (top) cloud-filtering enabled (FRESCO+ cloud fraction $> 20\,\%$) and (bottom) disabled on 18 December 2007. A plume associated to a long-range transport event (following a cyclone) can be seen south of Greenland only in the non-filtered data.

- Little light penetrates to the atmosphere below the cloud and even less gets transmitted again to the satellite, which leads to a relatively small and stable block air-mass factor for the atmosphere between surface and cloud (shielding effect).

These effects are illustrated in Fig. 2.

Further interesting effects can occur when clouds reside over bright surfaces (snow and ice). Due to the high reflectivity of the surface, not much light is absorbed there. Instead, light between the surface and the cloud bottom will continually propagate back and forth until it finally penetrates the cloud and reaches the instrument. This leads to a vastly increased light-path and can lead to an increased block air-mass factor below the cloud due to the cloud's presence. This effect is hard to find in satellite data, as typical observation geometries over bright scenes allow only for a mitigation of the shielding effect, not an absolute enhancement of the air-mass factor. It may, however, lead to an overestimation of NO_2 content when plumes are observed over sea-ice.

To take the effect of clouds on the radiative transfer into account, we first divide each satellite pixel into a cloudy and a cloud-free fraction, thus obtaining a geometric cloud fraction (CF). We obtain this cloud fraction by modeling the reflectivity of the pixel both under clear conditions and under cloudy conditions (with assumed cloud properties). The re-

flectivity R is derived from nadir measurements and solar irradiance at 437.5 nm

Then, the cloud fraction is obtained by modelling the observed reflectivity from the combined reflectivity of cloudy and clear part, similar to the method described in Wang et al. (2008), but using directly the wavelength range in which we retrieve NO_2 optical depths.

$$\mathrm{CF} = \frac{R_{\mathrm{obs}} - R_{\mathrm{cloud-free}}}{R_{\mathrm{cloudy}} - R_{\mathrm{cloud-free}}} \tag{3}$$

This is a simple approach. It is quick and robust and operates directly in the wavelength we are interested in, $437.5\,\mathrm{nm}$, where the most relevant absorption features are located. It is thus representative of the impact clouds have on the retrieval of NO_2 for this study. There are many other cloud retrievals operating on GOME-2 data, none of which operate on the spectral band used for retrieval of NO_2. A comparison to FRESCO+ cloud fractions shows that overall, the results of both cloud retrievals are very similar with a narrow band of scattering. Over bright surfaces and sunglint, larger deviations are possible.

Here, we use the monthly albedo climatologies based on MERIS data by Popp et al. (2011) to model cloudy and cloud-free reflectivities. Operationally, we obtain reflectivity values from a look-up table.

However, this yields only the geometric cloud fraction. For purposes of determining the air-mass factor, we need to use the radiance cloud fraction: the fraction of the radiation entering the detector that was influenced by clouds. This is obtained by weighting the cloud fraction with the modeled reflectivities. Usually, the cloud radiance fraction will be larger than the geometric cloud fraction, because cloud reflectivities are higher than surface reflectivities for all but very white surfaces with an albedo $\gtrsim 0.8$. This means, that even small cloud fractions have a strong impact on the air-mass factor.

Finally, we determine the air-mass factor by weighting the cloudy and cloud-free air-mass factor by the radiance cloud fraction:

$$\begin{aligned}\mathrm{AMF}_{\mathrm{total}} =& \mathrm{CF}_{\mathrm{radiance}} \cdot \mathrm{AMF}_{\mathrm{cloudy}} + \\ & (1 - CF_{\mathrm{radiance}}) \cdot \mathrm{AMF}_{\mathrm{cloud-free}}.\end{aligned} \tag{4}$$

Usually, the cloud-free air-mass factor is determined either from a standard atmospheric profile or from climatological simulations (like MOZART, Horowitz et al. (2003)). These cannot, however, be used for analysis of long-range transport events, as the NO_2 will typically be strongly localized in altitude (Rastigejev et al., 2010) and deviate from stationary conditions.

The air-mass factor depends on where in vertical direction the trace gas is situated. This effect becomes stronger when there are clouds in the scene. However, the precise altitude is not needed, as long as we know the position of the trace gas with respect to the cloud (see Fig. 2 and Kokhanovsky and Rozanov, 2009).

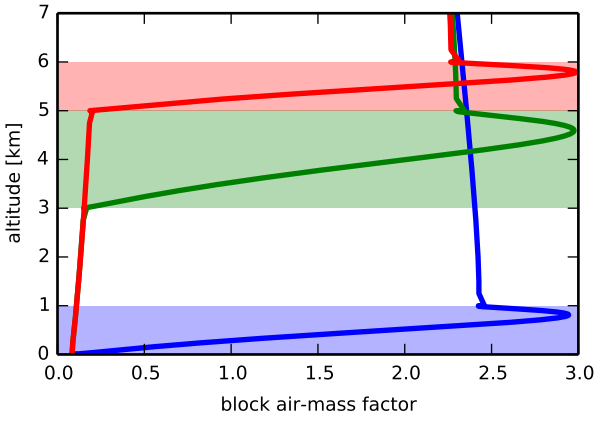

Fig. 2. Three exemplary block air-mass factors ($\lambda = 437.5\,\mathrm{nm}$) for scenes with clouds of optical thickness 20 at the respective shaded altitudes. Solar zenith angle and viewing angle are set to $0°$, the surface albedo is set to $a = 0.1$. The absolute altitudes of trace gas and cloud only have a small impact on sensitivity – the dominant effect stems from the relation of their respective altitudes.

Measurements from the TRACE-P campaign (Crawford et al., 2003) suggest that, for a long-range transport event associated with a cold front passing over an emission region, the trace gases (in their case CO) tend to be homogeneously mixed inside the cloud. It is possible that fractions of the trace gas content are also situated below or above the cloud due to the nature of convective processes, condensation and subsidence of liquid water droplets. In the absence of coincident in-situ observations of cloud properties and NO_2 profiles, model data can be used to investigate the relative positioning of the two quantities during long-range transport events.

We have used MACC-II reanalysis (Inness et al., 2013) liquid and frozen water content and NO_2 concentrations to find further indications of the relation in altitude between clouds and NO_2 for a prominent case of an NO_2 long-range transport event linked to clouds (Fig. 3). For beginning of October 2010 in Europe (detailed case study in Sect. 5.4), we find that profiles at three locations of the plume, corresponding to different plume ages, profiles of NO_2 concentrations and liquid and frozen water content are very similar with a strong overlap of high-content altitude ranges (Fig. 4).

This is a strong indication that at least in this occasion, our assumptions are justified and the modeled air-mass factor is roughly representative of the actual air-mass factor of our observations. However, this is only anecdotal evidence. We could not devise a simple way to systematically test our assumption on a large population of long-range transport plumes, as plumes found in GOME-2 data have to be identi-

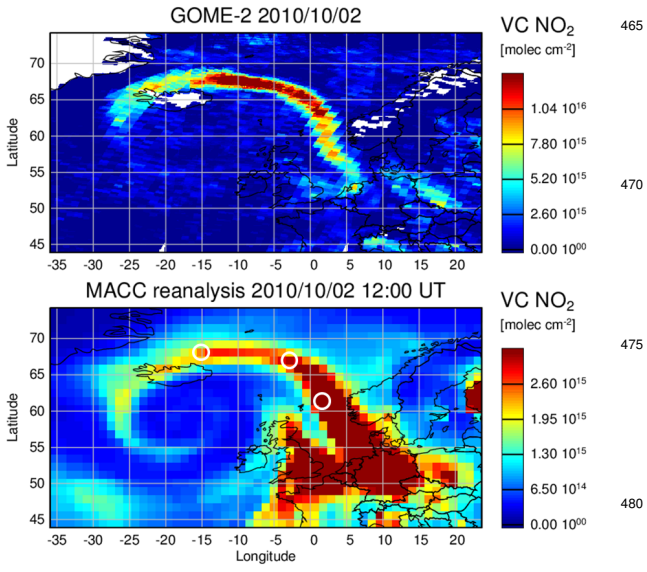

Fig. 3. Comparison of the NO_2 long-range transport plume near Europe on 02 October 2010 in GOME-2 and MACC-II reanalysis data. Note the difference in colorscale. White circles indicate the locations at which vertical profiles of NO_2 and water content were determined. The export is clearly visible in both satellite and model data. However, the model data show significantly lower NO_2 concentrations.

fied by hand in the model data and an objective comparison of vertical distributions is not a straight forward task.

Even though the results shown in Fig. 4 match our expectations, profiles of elevated NO_2 in model data have to be interpreted with caution as they are the result of parameterized convection which may not be adequate for all lifting scenarios and can introduce artifacts, e.g. when the maximum altitude is capped. Clouds in CTMs are devised from different parameterizations, and the relation of cloud and NO_2 altitude will depend on the details of the parameterizations used. While the model data examples shown support our approach, this aspect needs to be further investigated in the future, preferably with in-situ observations from aircrafts.

To quantify the uncertainties introduced by our assumptions, we performed a detailed analysis of the air-mass factor's dependency on radiation geometry and surface properties for varying relative cloud and NO_2 profiles. This analysis shows that if the NO_2 is well mixed inside the cloud, the errors of missing NO_2 slightly above or below the cloud are on the order of $\Delta\mathrm{AMF}/\mathrm{AMF} \lesssim 15\%$ (Fig. 5). This simplification holds, if most of the NO_2 is mixed inside the cloud.

If significant parts of the trace gas are situated above (or below) the cloud, we will underestimate (respectively overestimate) the air-mass factor. This effect is especially strong under non-nadir viewing and irradiation geometries. However, the effects of missing NO_2 above and below the cloud compensate each other for solar zenith angles of 40–$70\,^\circ$, which is the range most relevant for NO_2 long-range transport.

Based on these sensitivity studies, an NO_2 block profile that is homogeneously mixed inside the cloud and zero elsewhere is selected as the modeling hypothesis for both cloudy and clear sky air-mass factors. More specifically, we assume NO_2 to be homogeneously distributed between 3–$5\,\mathrm{km\,a.g.l.}$ and absent in all other parts of the atmosphere. If present, the cloud is modelled as extending over exactly the same altitude range. This approach is used for simplification and is only valid for long-range transport processes. During such processes, the exact altitude of the NO_2 content has little impact on the resulting air-mass factor as long as any NO_2 will be mixed inside a cloud, if present.

This leads to an inappropriate air-mass factor for regions with NO_2 close to the surface. Since long-range transport events will usually have elevated plumes of NO_2 and this study focusses only on NO_2 over the oceans, no regions with significant amounts of surface NO_2 will enter our further analysis. Thus, we effectively use this air-mass factor only for NO_2 long-range transport events.

A sensitivity study shows that from a broad sample of setups of surface and cloud properties, the 3–$5\,\mathrm{km\,a.g.l.}$ scenario is situated right in the center of the resulting air-mass factors (deviating by less than $1\,\%$ from the mean) over all occurring geometries (Fig. 8). The relative standard deviation of the resulting air-mass factors from the whole set of setups is less than $3\,\%$ over all viewing geometries.

The estimated tropospheric NO_2 vertical column density (VCD) is finally calculated by applying the combined cloudy and cloud-free air-mass factor to the tropospheric NO_2 slant column density.

The NO_2 product described here is used only for long-range transport analyses over the open ocean, where no concentrated NO_2 emissions take place.

3 Methodology

To detect long-range transport events in a global dataset spanning five years of observation, we implemented an algorithm to find, verify and assess plumes from long-range transport events.

3.1 Identification of potential long-range transport events

As a result of the short lifetime of NO_2 in the planetary boundary layer, observations from satellite show NO_2 to be strongly correlated to emission regions (Leue et al., 2001; Martin et al., 2002; Boersma et al., 2004; Richter et al., 2005; van der A et al., 2008). Long-time averages indicate emission and major outflow regions. NO_2 long-range transport events are isolated events that deviate from steady background pollution. During such an event plumes of NO_2 suddenly appear

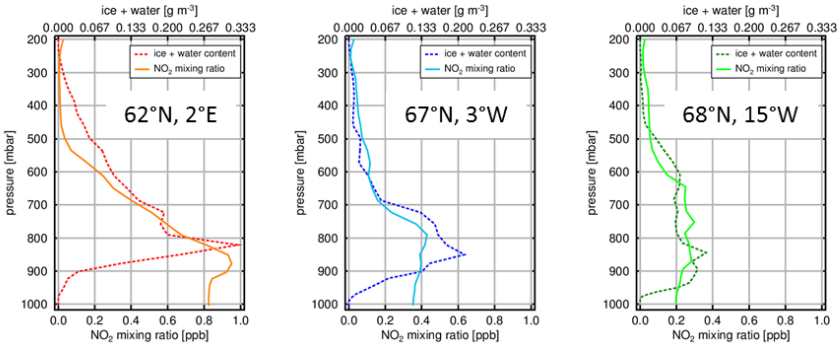

Fig. 4. Comparison of NO_2 mixing ratio and frozen and liquid water content from MACC-II reanalysis data for three locations (roughly corresponding to increasing plume age from left to right) in the plume shown in Fig. 3. The distributions are highly correlated, indicating that our assumptions of full mixing of NO_2 within a present cloud is justified.

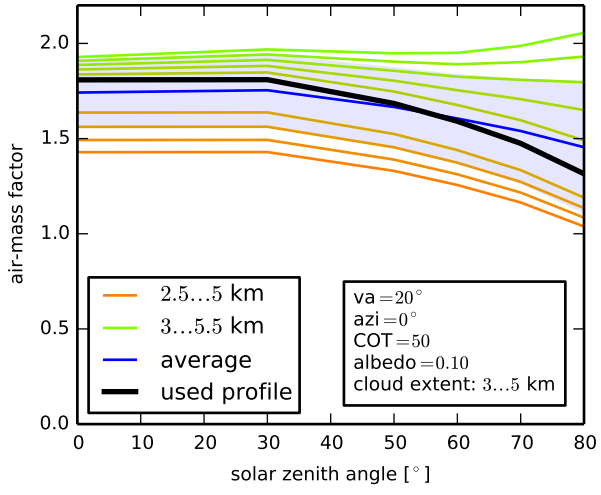

Fig. 5. Illustration of the air-mass factor dependency on the solar zenith angle for varying NO_2 profiles and an invariant cloud profile. The black line shows the profile used for this study. The ensemble average and the standard deviation are indicated in blue. We used a cloud vertical extent of $3\ldots5\,\mathrm{km}$, a surface albedo $a = 0.1$, a viewing angle $\mathrm{va} = 20\,^\circ$, relative azimuth angle $\mathrm{azi} = 0\,^\circ$ (forward direction) and cloud optical thickness $\mathrm{COT} = 50$ (as used for data analysis).

in the data and – if they persist long enough and observation conditions are favorable – move between subsequent observations.

Analysis of NO_2 long-range transport can be performed by just browsing through the data. For a more thorough and objective analysis, we need to enable computers to systematically find such events.

We therefore have developed an algorithm to identify intercontinental long-range transport events in maps of NO_2 vertical column densities. This algorithm builds on the following premises:

- long-range transport events are suddenly appearing and disappearing anomalies in the daily, global NO_2 observations
- long-range transport events show extended NO_2 plumes which are composed of at least two pixels of $0.5^\circ \times 0.5^\circ$
- long-range transport events can be traced back to source regions with lagrangian transport models

To ensure that we recognize sudden features in the global timeseries, we compute a sliding mean and standard deviation for each day, which includes a number n_{days} of observations before and after the day in question. We do not include the day itself to avoid self-referencing of the plume.

For all further analysis, we only consider measurements over the oceans and mask out continental data. The oceans with their low NO_x sources allow us to see plumes clearly, whereas we might easily miss them over the continents or interpret varying emissions or effects of meteorological conditions on NO_2 observations as long-range transport events. Plumes over the ocean can only result from transport processes, from artifacts in the observations or retrieval or from individual events such as large thunderstorms and or uncontrolled fires on oil platforms. NO_x emissions from lightning are rarely detected in satellite data, due to both small vertical column densities and unfavorable viewing conditions (Beirle et al., 2009). However, in some cases they can interfere with our retrieval as discussed in section Sect. 4.4. Emissions from both ships and aircraft are too regular and too small in absolute concentrations to appear as anomalous plumes in the data.

For each day, we select those pixels, which show NO_2 columns at least $n_{\mathrm{seed}} \times \sigma$ above the mean. These are the candidate pixels. All candidate pixels within a great-circle

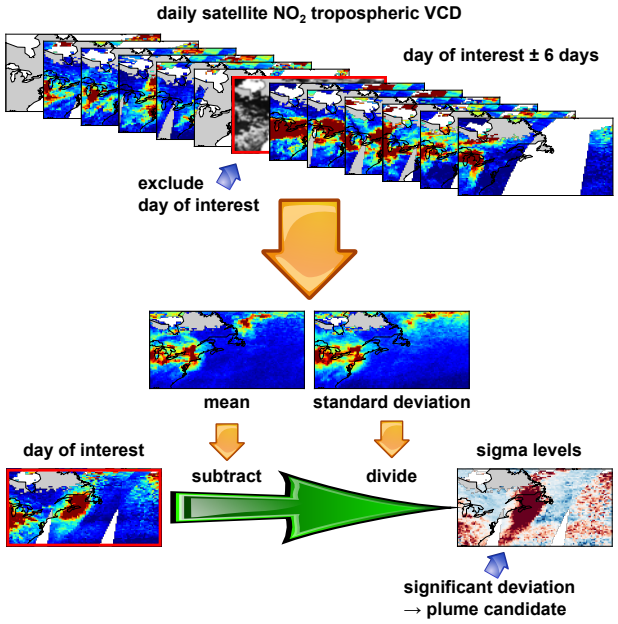

Fig. 6. Schematics of how GOME-2 satellite data is prepared in order to detect NO_2 long-range transport events. The observational data are compared to a sliding mean and standard deviation of the six days preceeding and following the day of observation. Strong positive anomalies in NO_2 vertical column densities are selected as potential for long-range transport plumes.

distance $\Delta\theta$ of another pixel become seeds. All seeds within a distance of $\Delta\theta$ are merged. Pixels that have no neighbor within $\Delta\theta$ are discarded as outliers. The preparation of GOME-2 data is illustrated in Fig. 6. The further processing of these data to detect, assess and verify plumes is shown in Fig. 7.

These seeds – containing two or more pixels – are now grown: all adjacent pixels which are at least $n_{\mathrm{member}}\sigma$ above the mean are merged into the seed to form the plume. We iterate this process until no further pixels match the criteria. We discard all plumes that include less than $n_{\mathrm{min,molec}}$ molecules of NO_2 for computational purposes and to filter out false positives from noise in the data.

For our analysis, we chose the following constants: $n_{\mathrm{days}} = \pm 6$, $n_{\mathrm{seed}} = 3$, $n_{\mathrm{member}} = 2$, $\Delta\theta = 1.0°$, and $n_{\mathrm{min,molec}} = 5 \times 10^{30}$molecules.

3.2 Backtracking of potential long-range transport events

Long-range transport events are dynamic processes. We perform backtracking of the plumes identified in the previous step. Then, we assess the properties of the plumes – in particular their altitude and origin – and discriminate between actual long-range transport events and artifacts from incomplete removal of stratospheric NO_2, instrument noise, or diurnal variation.

We employ the HYSPLIT_v4 lagrangian transport model (Draxler, 1999; Draxler and Hess, 1998, 1997) and supply it with Global Data Assimilation System (GDAS) (National Climatic Data Center, NESDIS, NOAA, U.S. Department of Commerce) meteorological data as input. For each plume, coordinates of all the associated pixels are inserted into HYSPLIT as starting points of back-trajectories. We do this at multiple altitude levels as we do not have any altitude information on the NO_2 itself from the observations. FRESCO+ cloud top height (CTH) can be used to verify our assumptions about the vertical relationship between NO_2 and cloud, but we chose not to use it for determining the altitude of the NO_2, so that a potentially incorrect assumption in the air-mass factor calculation does not lead to an exclusion of the real backtrajectory.

We select altitudes from $1000\,\mathrm{m}$ to $6000\,\mathrm{m}$ in steps of $500\,\mathrm{m}$. HYSPLIT is then run backwards for 120 hours – a little more than the reported NO_2 lifetime of up to several days in the free troposphere (Wenig et al., 2003) – and all the snapshots of the plumes (all associated points at 120 time steps and 11 altitude levels) are recorded.

For each of these snapshots we retrieve the seasonal mean tropospheric NO_2 vertical column density for each point that is within the planetary boundary layer (assumed to reach up to $1000\,\mathrm{m}$). We obtain these values from the seasonally averaged cloud-free GOME-2 data from 2007 to 2011, gridded to the same resolution as the data used for plume retrieval. Pixels in the seasonal average that are hit by multiple backtrajectories are included multiple times, leading to a weighting of sources. A value of zero is recorded for points above the boundary layer. These values serve as a measure of the pollution which is available for transport at this point of the backtrajectory.

We compute a simple score for each snapshot to select the most likely source of the plume. This score implicitly favors a low dispersion of the points and thus also a young plume. It is computed as the number of trajectories that reside in the continental planetary boundary layer (below $1000\,\mathrm{m}$a.s.l.) for every time step in the backtrajectory (snapshot).

We select the snapshot with the highest score to mark the beginning of the transport event and discard all snapshots from other altitudes and from all timesteps that go further back in time, leaving us only with the preferred trajectory.

As we derive both the altitude of the plume and the origin from this analysis, there may be ambiguities in the results. Backtrajectories from multiple altitudes may lead to the same or different source regions. While this is rather uncommon, when inspecting results, it may affect parts of the results. Also, it is possible that occasional NO_2 plumes that do not belong to a long-range transport event are falsely assigned a backtrajectory to a source region. We do not have a way to discriminate between these cases. However, we have

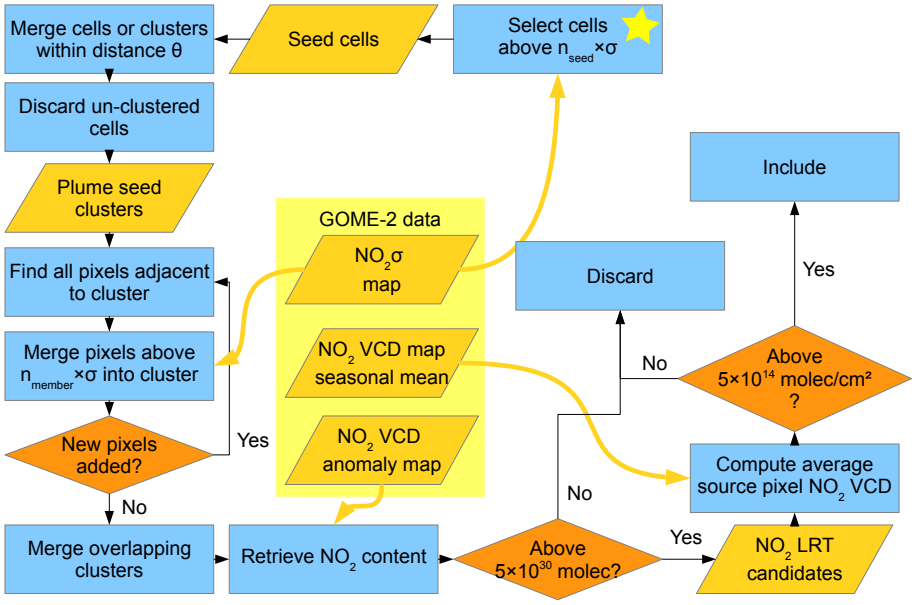

Fig. 7. Schematics of how long-range transport plumes are detected using our algorithm, starting from the prepared GOME-2 data as shown in Fig. 6.

inspected backtrajectories of randomly selected events from our results and most backtrajectories are plausible.

3.3 Verification of potential long-range transport events

After we have determined the most likely trajectory, we assess whether or not this is actually a long-range transport event. We sum up the average seasonal clear-sky NO_2 vertical column density at the beginning of the trajectory of each pixel in the plume. The ratio between this measure of NO_2 pollution in the determined source region and the number of pixels in the plume has to exceed a minimum value in order to verify this plume as belonging to a long-range transport event. Effectively, this determines the average source region NO_2 vertical column density for this plume.

We demand that the source region pollution averaged over all pixels in the plume exceeds $5 \times 10^{14} \mathrm{molecules/cm^2}$ for a credible long-range transport event. This criterion is based on manual fine-tuning to find an optimum balance between obvious false positive and false negative events, by browsing through the results. All plumes that do not fulfill this criterion are discarded. Roughly 56% of all plumes are discarded by this criterion.

This method is feasible because we analyze plumes only over the ocean and assume that all source regions are located on the continents. While emissions from ships, airplanes and lightning contribute to the overall NO_2 budget, they are associated with significantly lower NO_2 vertical column densities than continental emissions, with an observed NO_2 vertical column density on the order of $10^{15} \mathrm{molecules/cm^2}$ for the most polluted shipping lanes (Franke et al., 2009). Due to stray pixels in the backtrajectories and the large spacial extent of NO_2 long-range transport events, this local concentration is not enough to qualify shipping lanes as origin of long-range transport by the above criterion, due to the averaging process.

3.4 Assessment of properties

The aforementioned method allows us not only to identify transport-related NO_2 plumes but also to derive a number of properties for each individual long-range transport event. These properties include:

- the total area encompassed by the plume (from the extent of the pixels)
- the NO_2 content in each pixel (excess tropospheric NO_2 vertical column density above the sliding mean)
- the total NO_2 content in units of molecules or mass in GgN (by summing up vertical columns over the plume area)
- the source region of the plume
- the age of the plume since it left the boundary layer
- the altitude evolution of the plume from emission to observation
- the horizontal velocity of the plume

In some cases, it is possible to identify the same plume at earlier or later time steps in the satellite data to get a more detailed analysis of such an event. Currently, we need to do this manually and therefore limit this part of the analysis to selected case studies.

4 Limitations

To apply the method outlined in the previous section, we have to limit the analysis to favorable conditions and assume simple long-range transport scenarios. There are a number of factors which contribute to the overall uncertainty of our developed method.

4.1 Satellite data

NO_2 observations from satellite are prone to retrieval errors, when trace gas absorption cross sections are fitted to the spectral radiance to retrieve the slant column density. With regard to the fit residual, we estimate the errors for an individual pixel to be on the order of $5 \cdot 10^{14} \mathrm{molecules/cm^2}$ in equatorial regions, which amounts to up to a few percent. Plumes have to exceed an NO_2 content of 5×10^{30} molecules to be included in our study, which typically amounts to tens or hundreds of polluted pixels. This, together with the regridding of the data, partially mitigates the uncertainties.

The GOME-2 instruments measure only in daylight and cannot observe NO_2 during winter at higher latitudes. This impedes the analysis of long-range transport events traveling to the Arctic, one of the most sensitive areas of interest for the long-range transport of air pollution (Sodemann et al., 2011).

4.2 Air-mass factors

To obtain NO_2 vertical column densities, we assume a profile that locates NO_2 between 3–5 km in altitude. Sensitivity studies show that the results for the NO_2 air-mass factor do not vary strongly within this altitude range (Fig. 8) if it is well mixed within the cloud or elevated from the surface in the absence of a cloud. The standard deviation of air-mass factors for 2 km thick layers of NO_2 mixed inside clouds for different altitudes is on the order of 3 % for typical observation geometries. Variations of the thickness of the cloud and NO_2 layer have a similarly small effect.

Based on Crawford et al. (2003), we assume that the trace gas will be homogeneously mixed inside any cloud that may be present and stretch over an altitude range of 3–5 km during a long-range transport event. Our sensitivity studies show (Fig. 5) that the air-mass factor displays only small variance when a fraction of the trace gas is present above or below the cloud, as long as the majority is mixed inside the cloud. For this study, we chose the assumptions such that they produce the values near the center of the air-mass factors of all plausible NO_2-cloud-distributions.

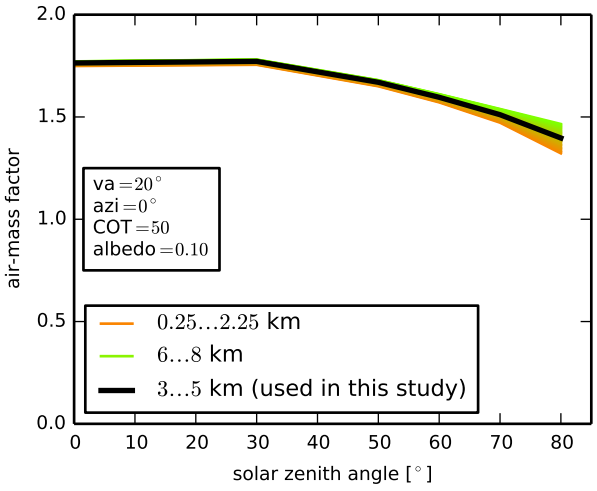

Fig. 8. Sample air-mass factor dependency on solar zenith angle for NO_2 fully mixed inside clouds at varying altitudes. The black line indicates the cloud and NO_2 profile used in this study. We used a surface albedo $a = 0.1$, a viewing angle $\mathrm{va} = 20°$, relative azimuth angle $\mathrm{azi} = 0°$ (forward direction) and cloud optical thickness $\mathrm{COT} = 50$ (as was used for data analysis).

Due to the lack of reliable information on the cloud profile (cloud retrievals typically only yield the cloud top and bottom heights), we use a homogeneous profile. We do not take the effects of aerosols explicitly into account, as long-range transport plumes tend to travel at elevated altitudes. This eliminates the effects of sea-spray. The effects of other aerosols should partially be mitigated by our cloud product. The remaining effect should be on the order of less than a few percent.

We do not take into account multi-layered clouds. In most cases, these would reduce the NO_2 signal and leave the plume or parts of it undetected by our algorithm. If NO_2 mixed inside a cloud would reside above another cloud, this could lead to an overestimation of NO_2 vertical column density due to an elongated light-path. This is not likely as most plumes tend to reside at relatively low altitudes.

4.3 Plume retrieval

The results of the long-range transport plume retrieval algorithm depend on its input parameters. The chosen thresholds and averaging windows are a result of manual inspection of satellite scenes and comparison to the results from the retrieval.

There are several parameters of interest:

- the σ-levels chosen for seed pixels and member pixels of a plume
- the time frame for the sliding mean calculations

– the maximum distance at which plumes are merged (i.e. the minimum distance of two distinct plumes)

Sensitivity studies show that the results are relatively stable with regards to these parameters. The used parameter sets were chosen to allow deriving a good result in reasonable computation time. Increasing the minimum distance between two distinct plumes will lead to slightly more plumes with high masses.

After plumes are retrieved, varying selection criteria for the preferred backtrajectory and varying verification criteria for the plume will lead to slightly different results. We have therefore implemented criteria that are as simple as possible while producing results that are consistent with manual inspection of a range of sample plumes.

The Lagrangian transport simulations we perform for each plume are also affected by uncertainties. Due to the coarse resolution of the used meteorological and NO_2 data – both vertically and horizontally – individual pixels will eventually diverge from the bulk in case of chaotic movement under conditions with strong winds. This is especially true for old plumes which provide the least reliable data. In most cases the bulk of the plume will stay relatively close together along the backtrajectory.

Occasionally, a sudden emission of NO_2 over the ocean may also be classified as long-range transport event by our algorithm, when backtrajectories to a prominent emission region exist. This could only be avoided by cross-referencing events with a catalogue of such oceanic emission events.

We do not take plumes over the continents into account. There, fluctuating sources, albedo and topography make the analysis of continental long-range transport challenging. When we limit the analysis to the ocean, we have a data set that is much easier to interpret. However, we are prone to losing parts of plumes which are just on the shore. We also do not detect any continental plumes which do not move onto the ocean.

4.4 Lightning NO_x

There is another source of NO_2 over the ocean: lightning (Beirle et al., 2004). Schumann and Huntrieser (2007) report that approximately $5 \pm 3\,\mathrm{TgN/a}$ may originate from NO_x emitted by lightning ($LiNO_x$). Ott et al. (2010) show that NO_x concentrations in thunderstorm clouds may be higher than $10\,\mathrm{ppbv}$. They also show that only a small fraction of this $LiNO_x$ is located in the cloud top, where the sensitivity of satellite observations is high. Instead, most of it is located in the lower parts of the cloud or below the cloud, where the sensitivity of satellite observations is low.

For this study we tried to locate major plumes of $LiNO_x$ found in MOZAIC data (Sauvage et al., 2011). Only a very small fraction of these events was found in corresponding SCIAMACHY NO_2 satellite data, which was processed in the same way as the GOME-2 data in this study.

Additionally, the verification using backtrajectories makes it unlikely that $LiNO_x$ plumes are classified as long-range transport events in this study. Wenig et al. (2003) report that in their NO_2 long-range transport study, $LiNO_x$ is likely to contribute to the total NO_2 content, but is most likely not the only or dominant source.

However, low-pressure regions – which turn out to foster long-range transport – are often linked to thunderstorms which will produce $LiNO_x$, thereby creating a higher probability of lightning NO_2 contamination of our data. As there is no way to unambiguously distinguish NO_2 from lightning and transport over the ocean in satellite data, this is an additional source of uncertainty in our estimates.

5 Case studies

To illustrate the nature of NO_2 long-range transport events and the successful application of the detection algorithm, we have selected four prominent samples from the collected set of events to scrutinize them in detail.

We use data from the NCEP/NCAR Reanalysis Project (Kalnay et al., 1996) to investigate meteorological conditions that accompany detected long-range transport events. Detailed properties of the plumes occurring during long-range transport events (for each observation) are given in Table 1.

5.1 North Atlantic, 17–19 December 2007

Fig. 9 shows a striking example of an NO_2 long-range transport event in the western North Atlantic from 17 to 19 December 2007. Unfortunately, GOME-2 was operated in narrow-swath mode on 16 December 2007, so that we cannot observe how the plume separates from its emission region while being uplifted during the course of this day.

The NO_2 plume originates from the East Coast of North America, near the major emission regions of New York, Boston and Chicago. It closely follows the center of a rapidly developing low-pressure system crossing the region from south-west to north-east. After two days, it crosses Newfoundland and subsequently disappears near Greenland in the Arctic night where GOME-2 cannot observe NO_2 vertical column densities. The origin and transport direction of this NO_2 long-range transport event are typical for this region and lie within the major storm track to the East of North America (Whittaker and Horn, 1984).

This mechanism of NO_2 long-range transport has been analyzed in a case study by Stohl et al. (2003). Unlike that study, here the NO_2 is centered on the cyclone as seen in NCEP DOE AMIP-II Reanalysis mean sea level pressure data. When we inspect further prominent long-range transport events emitted from the North American East Coast, we find that the NO_2 plumes typically follow a rapidly forming cyclone.

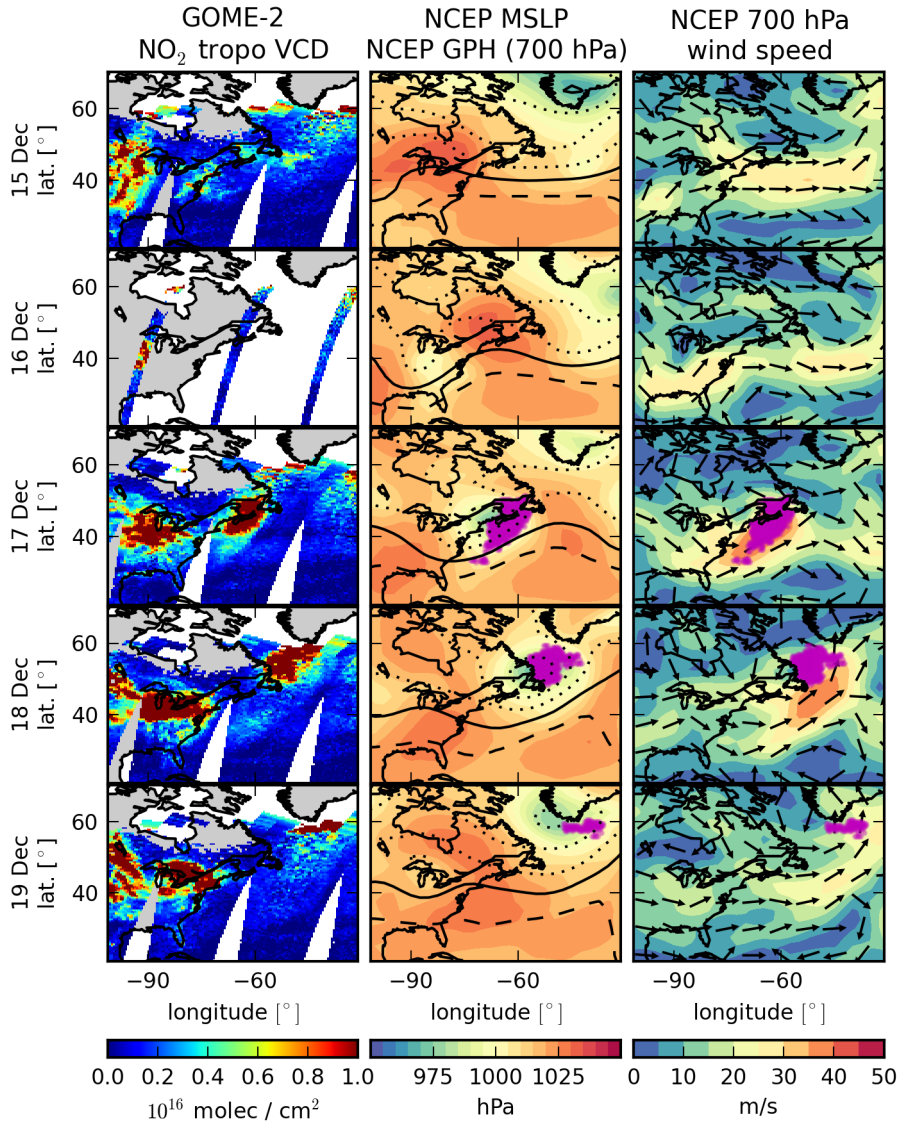

Fig. 9. Timeseries of the days preceding and during a long-range transport event over the North Atlantic on 17 to 19 December 2007. The locations of satellite pixels identified as belonging to the long-range transport plume are indicated by purple circles in the center and right columns. Shown are (left) the GOME-2 NO_2 tropospheric vertical column density, (center) the NCEP DOE AMIP-II Reanalysis mean sea-level pressure (colors) and geopotential height at 700 hPa (contours) and (right) horizontal wind speeds at 700 hPa (amplitude and direction). For geopotential height, the solid line denotes 3 km, dashed / dotted indicate higher / lower geopotential height in steps of 125 m. A low pressure system is quickly evolving into a cyclone. It elevates an NO_2 plume – as seen in its backtrajectories – and transports it towards Greenland.

Such clear and long-lasting long-range transport events that can be observed for three consecutive days in GOME-2 data are rare. The reason for that lies in the combination of prerequisites for long-range transport, their typical routes and the specifics of DOAS satellite observations:

- most long-range transport events form in the local winter because emission rates are high, low pressure systems are common, and NO_2 lifetime is long
- long-range transport events tend to move polewards, if they do not dissolve

This means that many long-lasting plumes will quickly move out of sight of the satellite instrument which cannot observe NO_2 in or near regions of polar night.

From our observations, we estimate the plume to contain roughly $2.31\,\mathrm{GgN}$ on the first day of observation. From the backtracing of the long-range transport event, we estimate the plume to be about 50 hours old (since detaching from the planetary boundary layer) at the time of first observation. If we take photochemistry and dilution of the plume in the first 50 hours into account, the amount of nitrogen exported from the continent in this event may have been significantly larger. Unfortunately, the few samples do not even allow to determine a rough estimate of the lifetime of NO_2 in this event.

The plume is transported at an altitude between $1.0\,\mathrm{km}$ on the first and $2.0\,\mathrm{km}$ on the last day of observation, as retrieved from the backtrajectories. FRESCO+ cloud top heights (CTH) for these measurements are derived to lie in the range of $840 \ldots 650\mathrm{hPa}$, corresponding roughly to $1.4 \ldots 3.5\,\mathrm{km}$. This is consistent with the retrieved altitudes, which do not neccessarily denote the top of the NO_2 distribution (and thus the cloud), but the altitude from which most trajectories lead back to a source region which could be assumed to lie in the center of mass of the vertical distribution. The FRESCO+ CTH varies over the extent of the plume by roughly $200\mathrm{hPa}$ which may indicate that the altitude of the NO_2 is not homogeneous over the plume.

Further properties of the event are summarized in Table 1. We derive the minimum average travel speed of the plume (the actual speed will be higher due to curved trajectories) from these properties, which amounted to $59\,\mathrm{km/h}$ from the first to the second observation. On the next day, we can only calculate a lower limit ($32\,\mathrm{km/h}$) due to the cut-off at polar night.

Fig. 10 illustrates how closely the trajectory obtained from the backtracing algorithm matches the satellite observations of the plume at earlier times, even though all observations of an NO_2 plume are handled independently. Due to the coarse horizontal, vertical and temporal resolution of the meteorological data, the trajectory is not accurate on the outer rim of the plume; there, trajectories diverge from the main path.

5.2 South Africa, 9–12 July 2008

In the Southern Hemisphere, South Africa is the only region regularly emitting NO_2 long-range transport events. A clear event can be seen in the satellite data from 09 July 2008 emitted from the industrial region on the Highveld plateau. It follows the winds in the free troposphere towards the East for several days, disappearing after its last observation on 12 July 2008 near the Australian West Coast (Fig. 11).

South Africa has ideal conditions to create and observe long-range transport events. The Highveld plateau concentrates the nation's industry, injects factory and power plant exhausts at altitudes of more than $1,500\,\mathrm{m}$ into the atmosphere, and is an isolated emission region. The prevailing north-westerly winds in this region propel elevated plumes onto the open ocean, which makes it easy to observe them with satellite measurements.

The World Wide Lightning Location Network (WWLLN) finds a significant amount of lightning strikes in the area where the plume is observed on 09 and 10 July 2008 (Fig. 12). On the following days, the – then weaker – thunderstorm and the NO_2 plume are no longer co-located and further impact on the NO_2 plume can be excluded. With our detection algorithm, we cannot distinguish NO_2 from anthropogenic sources and $LiNO_x$ other than by location and trajectory. We cannot tell if this observation actually shows a long-range transport event or $LiNO_x$ or both. It is possible though unlikely, that the observed plume is not anthropogenic in origin, but rather originates in the strong thunderstorm and is then transported further downwind. In that case, it is not clear, why the NO_2 plume and the thunderstorm would separate. It appears more likely that the strong thunderstorm will replenish the NO_2 content of the plume, thereby enhancing its observed lifetime.

It is plausible that long-range transport events will occasionally be accompanied by thunderstorms. These may in turn lead to an enlarged NO_2 content or to an apparent longer lifetime of NO_2 inside the plume. From our efforts to observe $LiNO_x$ in reported strong thunderstorms and their distinguished seasonal and geographical distribution (Sect. 6.2), however, it appears that thunderstorms will not be the single cause for most of the observed plumes.

This plume bears similarities to the one analyzed by Wenig et al. (2003). The plume they observed crosses the ocean and arrives at Australia within five days which is consistent with the four consecutive observations in our data. They find thunderstorms with lightning coinciding with the plume on two observations, but the $LiNO_x$ alone could not explain the observed NO_2 vertical column densities in the plume. It might, however, have replenished the plume and thereby increased its apparent lifetime.

The selected long-range transport event is associated to a weak cyclone heading into the Antarctic. A cold front lifts the NO_2 plume up and their trajectories diverge subsequently. Winds of the free troposphere carry the plume straight to Australia.

We do not observe the plume entering Australia on 13 July 2008 due to a gap in the data and we do not find any traces of it on the following days. Upon arriving on shore the NO_2 may have descended and – due to shorter lifetime in the planetary boundary layer – dissipated. Also, rain may have washed out the NO_2 as HNO_3.

Due to the extent of this event, data gaps cover parts of the plume. This could explain why the measured NO_2 content of the plume increases from the first to the second day of observation. Other mechanisms to increase the observed NO_2 content are $LiNO_x$ production and conversion of reservoir species.

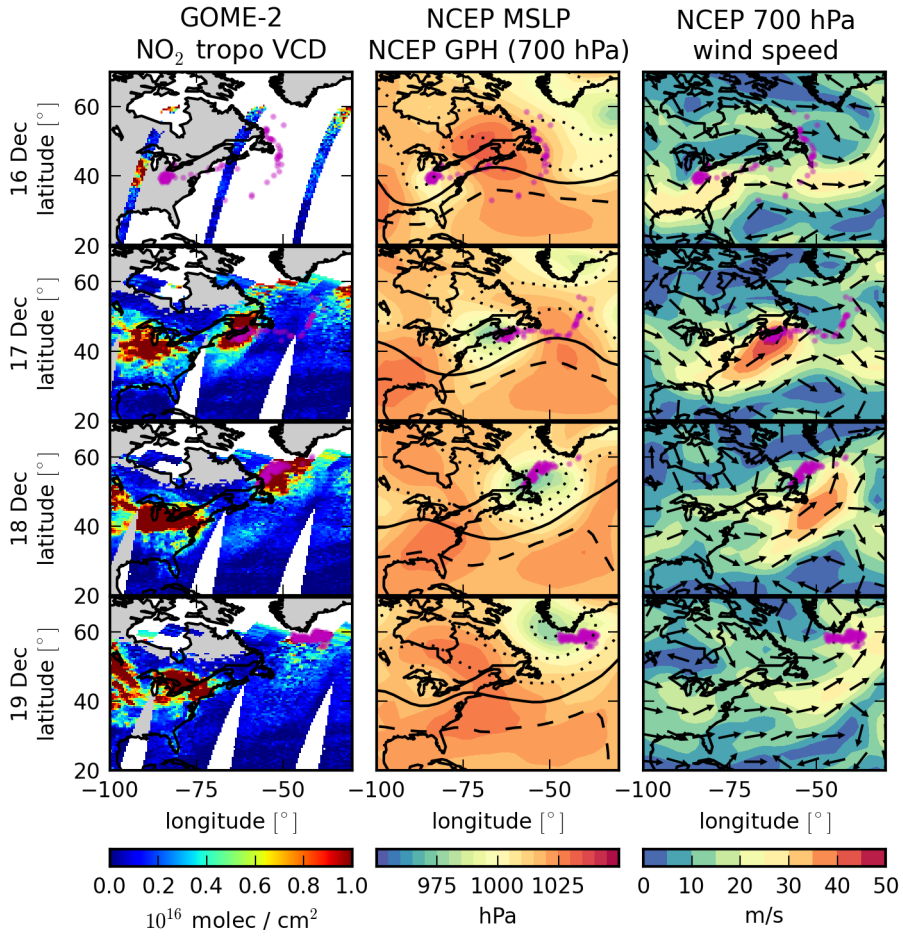

Fig. 10. Illustration of the backtrajectory of the last observation of this long-range transport event (19 December 2007). Data as in Fig. 9, but purple circles indicate the locations of the backtrajectories of the plume from 19 December 2007 at the respective dates. The plume detected on 19 December 2007 is only partially visible due to polar night. This becomes evident when comparing the backtrajectories on earlier dates with the observed NO_2 vertical column densities.

From the first to the second day of observation – while the plume follows the cyclone track – the average traveling speed is roughly $97\,\mathrm{km/h}$. After the plume and the cyclon decouple, the plume only travels at $59\,\mathrm{km/h}$ and $51\,\mathrm{km/h}$ on consecutive days.

Simulations with FLEXPART (Stohl et al., 2005), a more sophisticated lagrangian transport model, show the plume in their analysis to be traveling at altitudes from 2–$6\,\mathrm{km\,a.m.s.l.}$ after it separated from the emission region in the Highveld plateau, which is consistent with our assumptions. In FRESCO+ data, the CTH varies between $750\ldots500\mathrm{hPa}$ on the 10 July 2008, corresponding roughly to cloud top altitudes of $2.3\ldots5.5\,\mathrm{km}$. This is a bit lower than the estimated plume height of $6\,\mathrm{km}$ on this date, but consistent with the following observation. Both indicators point at an elevated plume in the free troposphere.

5.3 Australia, 27–30 April 2008

Australia only emits very few NO_2 plumes due to its limited emission sources, as compared with more populated and more heavily industrialized parts of the globe. However, we find a very long lasting long-range transport event in the data from 27–30 April 2008 which follows stationary wind patterns between a high-pressure system East of New Zealand and a low-pressure system over Antarctica. The plume disperses over the South Pacific ocean between two high-pressure systems (Fig. 13).

The size of this plume suggests that it could be caused by emissions from Australian bush fires. However, MODIS fire count data indicate that there were only few fires in South East and South West Australia. Most strong bush fires were located in North Australia and it is questionable if the short

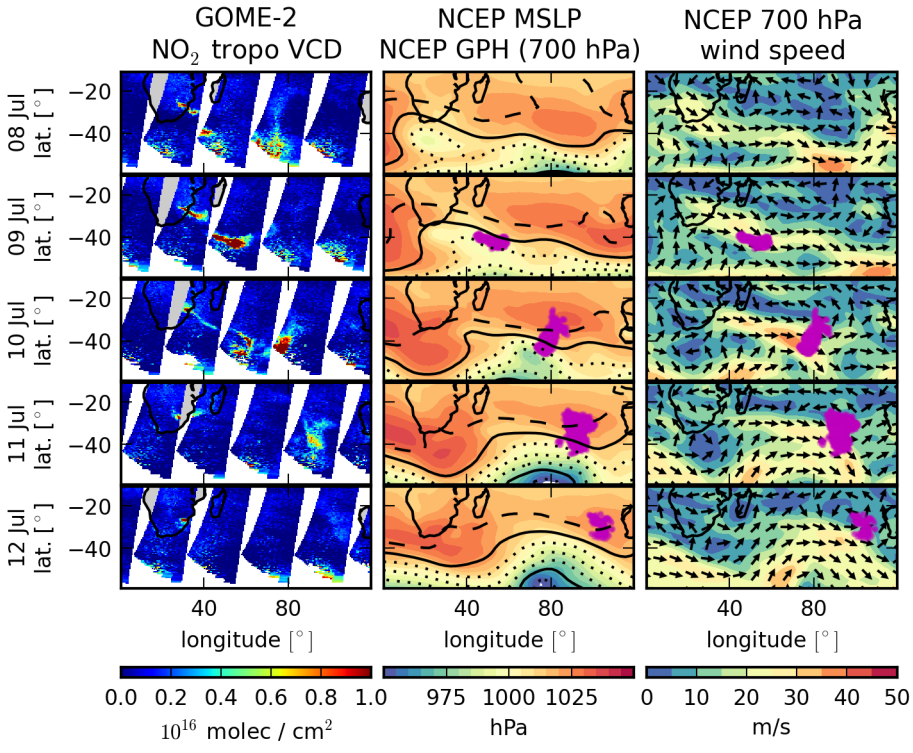

Fig. 11. As for Fig. 9, but showing a long-range transport event emitted from South Africa in July 2008. The NO_2 plume is transported from South Africa to the West Coast of Australia.

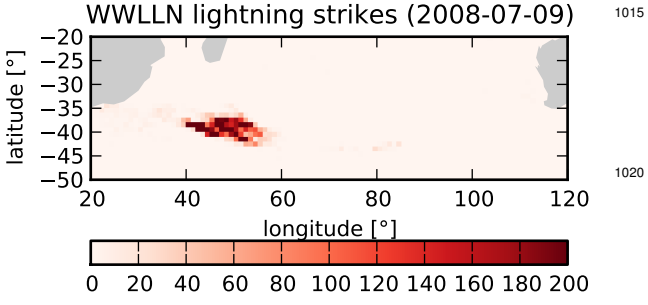

Fig. 12. Number of lightning strikes on 10 July 2008 observed with WWLLN over the ocean near South Africa. The lightning strikes are colocated with the observed position of the NO_2 plume (Fig. 11). Likely, this thunderstorm replenished the NO_2 content of the plume. On the following days, the thunderstorm produces significantly less lightning strikes and is no longer colocated with the transported plume.

lifetime of the NO_2 in these tropical latitudes would have allowed such a long transport.

Backtrajectories of the event indicate that the NO_2 may originate from the bush fires of both South East and South West Australia. NO_2 and glyoxal (CHOCHO) from large bush fires such as the Black Saturday fires are routinely observed in satellite data (Wittrock et al., 2006; Vrekoussis et al., 2009) and GOME-2 data show elevated NO_2 vertical column densities over southwestern Australia on 25 and 26 April 2008 – on the order of $3 \cdot 10^{15}\,\mathrm{molecules/cm^2}$, a factor two higher than background levels. It is likely, that our data product underestimates these values due to a lowered air-mass factor in the presence of black carbon aerosol in bush fire smoke plumes (Martin et al., 2003; Leitão et al., 2010; Giles et al., 2012). An origin in bush fires would also explain the necessary lifting of the NO_2 from the planetary boundary layer into the free troposphere in the absence of a frontal system (see Labonne et al., 2007).

The plume shows an exponential decay in NO_2 content – with a lifetime of approximately 28 hours estimated from observations – even though parts of it are not visible in GOME-2 data. Extrapolating backwards to the time of emission, we estimate the NO_2 content to be about $10.5\,\mathrm{Gg\,N}$. Note, however, that the apparent lifetime of NO_2 in the plume is influenced by conversion to and from reservoir species (especially PAN) which are not observed in this study and may lead to an increased effective lifetime of NO_2. A detailed analysis of the lifetime of NO_2 in long-range transport events with

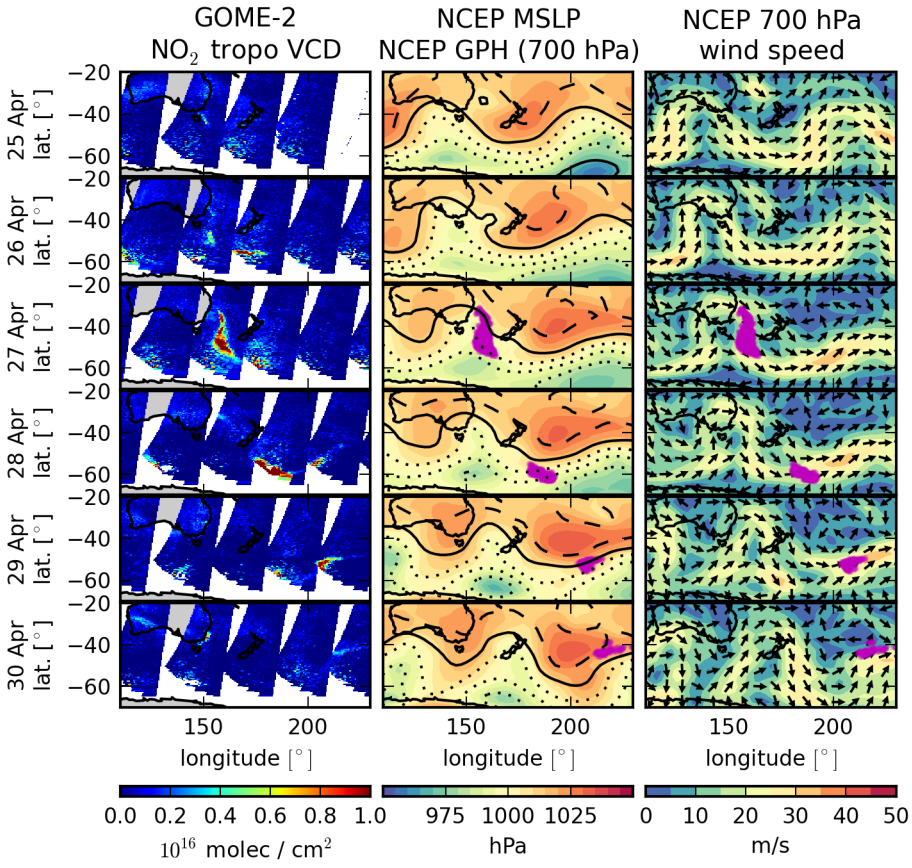

Fig. 13. As for Fig. 9, but showing a long-range transport event emitted in Australia in April 2008. The plume originates most likely from bush fires in Southwest Australia and follows the strong wind currents between highs over the Indian Ocean and lows over the Southern Ocean.

chemical sinks and sources is beyond the scope of this study and it is not clear if reservoir species will lead to shortened or to a prolonged observed lifetime of NO_2. Besides that, thunderstorms might lead to $LiNO_x$ replenishing the decaying NO_2 content of the plume.

Data from the Lightning Imaging Sensor (LIS, Christian et al., 1999; Christian, 1999) show a small thunderstorm off the coast of Australia on both 27 and 28 April 2008, coinciding with the plume only on 27 April. It appears that the movement of the plume and the thunderstorm are not linked to each other. On 28 April and subsequent days, the plume travels outside the latitude range observed by LIS.

This long-range transport event also shows deceleration over time. It starts with a minimum mean velocity of $105\,\mathrm{km/h}$ between the first two observations and decelerates to $74\,\mathrm{km/h}$ and $56\,\mathrm{km/h}$ on the consecutive days. This suggests that the NO_2 plume stays compact even after separating from the meteorological phenomenon leading to its emission.

5.4 Central Europe, 1–2 October 2010

Europe is a special case regarding long-range transport events. Due to local wind patterns, the NO_2 plumes are often ejected from the continent towards the north or north-west. Due to topography – strongly emitting regions located near the ocean in a bay – our algorithm retrieves very many long-range transport events here which are often very young at detection time.

On 1 and 2 October 2010 there is a prominent example of a long-range transport event in GOME-2 data. A small but elongated plume of NO_2 is emitted from the BeNeLux and Ruhr area when it is hit by a cyclone. The plume is transported onto the North Sea. It circles around the cyclone and is strongly filamented by the wind shear (see Fig. 14). On 3 October 2010 we can no longer identify the plume in the data. There is an apparent plume of NO_2 between Greenland and Svalbard, where observed NO_2 vertical column densities are highly variable. This anomaly is not detected in the algorithm as it shows no significant deviation above the sliding

mean observations and cannot be directly related to a long-range transport event.

The observations suggest that the NO_2 in the plume is transported towards the center of the cyclone. Due to the strong shear winds in the cyclone, the plume is dispersed by 04 October 2010. It was not detected by our algorithm and is hardly discernable in visual inspection of the satellite data.

6 Statistical analysis

In the previous section, we described and analyzed well-defined examples of long-range transport events detected by our algorithm which were also found by visual inspection of the data. With the developed algorithm, however, we have the opportunity to analyze a larger dataset and use the automated detection of long-range transport events to perform statistical analyses of this phenomenon over a longer period.

The analysis found a total of 3808 verified NO_2 long-range transport events (out of a total of 8626 events) in the GOME-2 data from 2007 to 2011. Fig. 15 shows their seasonal distribution for Northern and Southern Hemisphere. The distribution shows a strong seasonality in the frequency of long-range transport events; roughly half of all events occur during the local winter quarter. The Northern Hemisphere dominates the statistics due to more high-emission regions at higher latitudes.

We analyze the collection of long-range transport events from our algorithm to gain insight into favoring conditions, the hotspots and routes, and the range of parameters associated with them. First, we will focus on individual plumes' properties, then on ensemble properties.

6.1 Plume properties

Fig. 16 shows that the NO_2 content of the plumes roughly follows an exponential distribution function:

$$\mathrm{d}p(m) = \exp\left(-\frac{m}{m'}\right)\mathrm{d}m, \tag{5}$$

where m is the NO_2 content of the plume and m' the scale-mass of the distribution. A small scale mass indicates that small plumes dominate the distribution, while a large scale mass indicates that large plumes occur more regularly.

Looking only at the Northern Hemisphere (to exclude counteracting seasonality), we find that $m' = 0.25\,\mathrm{Gg\,N}$ for DJF, $m' = 0.24\,\mathrm{Gg\,N}$ for SON and $m' = 0.16\,\mathrm{Gg\,N}$ for MAM. Due to the low number of plumes, we could not determine m' for JJA. This means that plumes in autumn and winter follow a distribution that leads to much higher NO_2 content than in spring and (derived visually from Fig. 16) in summer. This supports cyclones and low temperatures as favorable conditions for long-range transport.

Further analysis reveals that this distribution is relatively stable across the five years investigated. We did not detect any significant trend in the mass distributions.

The observed NO_2 content distribution is a result of the NO_2 content distribution at the time of emission and the age distribution coupled with the lifetime of NO_2 in such events. Plumes observed on multiple days will appear multiple times in this statistic.

The estimated age of the plumes (Fig. 17) follows a distribution that appears to be the result from three independent effects:

- We find few plumes having ages of less than 24 hours, as not many plumes will have fully separated from their emission region in this short time period. They are thus still residing in the area of the emission region's outflow, where high NO_2 vertical column density variability impedes their detection.
- After the age distribution reaches a maximum at about 18 hours, the plume ages appear to be dominated by a decaying function which most likely results from dissociation, wash-out and dispersion of NO_2. This makes a detection by the algorithm less probable and incorporates a boundary between a plume and background NO_2.
- After about 96 hours, the distribution increases again. This is probably a bias resulting from our detection algorithm. A higher plume age increases the chance of backtrajectories hitting an emission region. This may lead to an increase in false positive detections for high plume ages.

The distribution partly resembles a cumulative distribution function, as individual plumes may be observed on multiple, consecutive days (see Sect. 5). Plumes with an age approximately $24\,\mathrm{h}$ apart might actually be observations of the same plume on consecutive days. This effect is corrected for in the regional statistics (Sect. 6.3).

The altitude distribution (Fig. 18) behaves as expected: all plumes less than a day old reside at low altitudes, near their emission region. The plumes shift to higher altitudes on the second day. After that, the distribution broadens as long-range transport events take different paths. The distribution suggests, that – to minimize systematic errors – we might improve our NO_2 vertical column densities by employing a lower altitude range for the calculation of reflectivities and air-mass factors – both in presence and absence of clouds. However, as we have shown the impact of this deviation is small.

Investigations into the distribution of the area encompassed by long-range transport plumes shows that plumes of an age of two to three days at observation time cover the largest area (not shown). This indicates that plumes start with high NO_2 concentrations and sharp boundaries, expand over

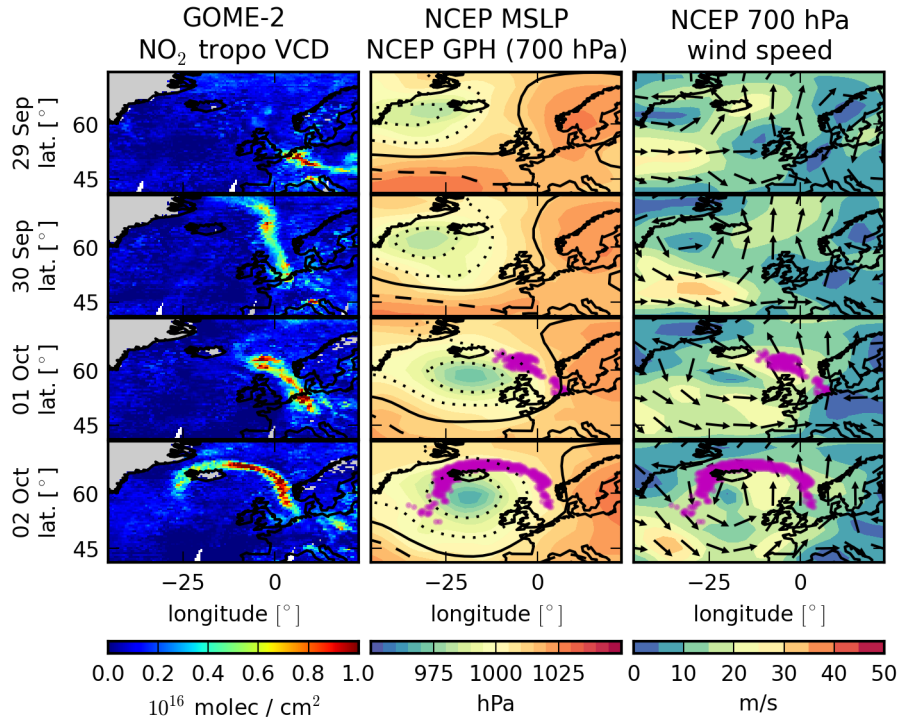

Fig. 14. As for Fig. 9, but showing a long-range transport event emitted in Europe in October 2010. The plume gets highly filamented when entering the cyclone. Note that the plume visible on 30 September 2010 separates from the rest of the plume and appears to have mostly been transported into the Arctic by 01 October 2010. Therefore, we do not include it in our analysis.

Table 1. Properties of NO_2 plumes observed during long-range transport case studies as estimated from GOME-2 data and HYSPLIT backtrajectories. For all plumes, properties (except for plume age) are derived only from the observational data for the given date – no information from prior or later observations is used.

Date	Plume Center		Altitude [km]	Age [h]	NO_2 content [Gg N]	Area [10^3 km^2]
North Atlantic						
2007-12-17	$45°N$	$63°W$	1.0	50	2.31	1093
2007-12-18	$55°N$	$52°W$	1.5	73	1.98	698
2007-12-19	$58°N$	$42°W$	2.0	95	0.65	207
South Africa						
2008-07-09	$42°S$	$53°E$	2.0	50	1.58	642
2008-07-10	$41°S$	$78°E$	1.5	73	1.74	1293
2008-07-11	$35°S$	$93°E$	6.0	96	1.40	1898
2008-07-12	$30°S$	$103°E$	4.5	119	0.39	881
Australia						
2008-04-27	$46°S$	$159°E$	4.0	47	1.83	1256
2008-04-28	$60°S$	$175°W$	1.0	69	0.89	311
2008-04-29	$52°S$	$152°W$	1.5	92	0.45	288
2008-04-30	$43°S$	$141°W$	3.0	115	0.16	319
Central Europe						
2010-10-01	$60°N$	$0°W$	1.0	21	0.38	372
2010-10-02	$64°N$	$11°W$	1.0	46	0.75	778

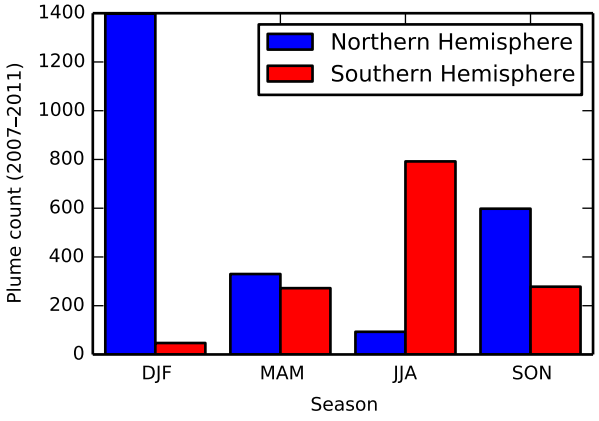

Fig. 15. Number of verified long-range transport plumes found by the detection algorithm in 2007–2011. There is a strong seasonality in both hemispheres, with a strong peak in local winter.

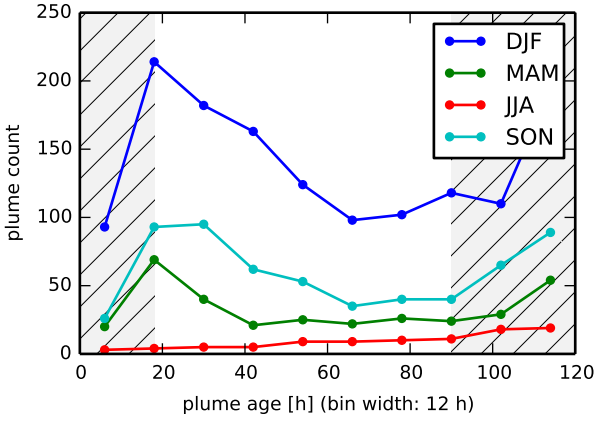

Fig. 17. Plume age at observation time of long-range transport events for 2007–2011, divided by season. The distribution illustrates the exponential decrease of long-range transport detections with age in the center. Two biases of the detection algorithm affect the hatched areas for low and high ages. See the text for details.

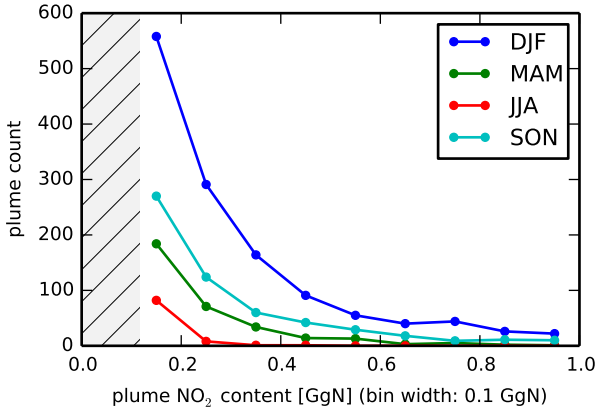

Fig. 16. NO_2 content of long-range transport events in the Northern Hemisphere, for different seasons. Note the lower mass limit of 5×10^{30} molecules (hatched area, corresponding to 0.12 Gg N).

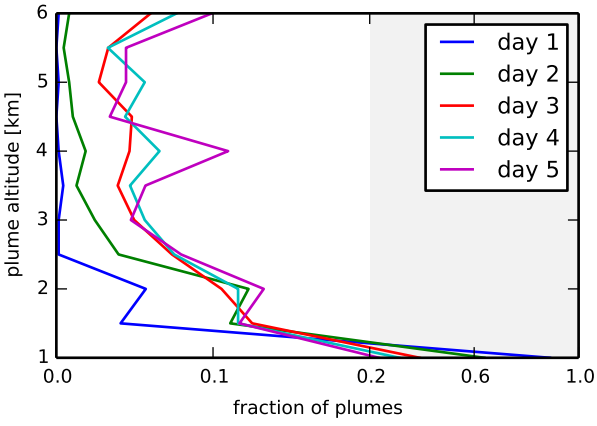

Fig. 18. Altitude distribution of NO_2 long-range transport plumes over the 11 altitude levels sampled in the HYSPLIT backtrajectories. Shown are the graphs for plumes younger than one day, between one and two days of age, etc. While most young plumes reside on the lowest level, they tend to distribute more equally in altitude over the following days. Note the compressed axis for fractions higher than 20 %.

a couple of days until the boundary of the plume gets blurred and the NO_2 content decreases.

6.2 Routes and sources

When browsing through the GOME-2 NO_2 data manually, long-range transport events tend to appear in particular regions and follow particular paths. With the derived dataset, we now verify this in a quantitative manner.

The first obvious analyses are the determination of the typical routes and their quantitative strength. To achieve this, we select the detected plumes from every day of observation and project their respective NO_2 content onto a global map. We sum up the NO_2 content from all plumes. This gives the total vertical column density of NO_2 in long-range transport events on a global map. Then, we divide by the total number of observations in the GOME-2 data set 2007–2011 for that particular grid cell ($0.5° \times 0.5°$). This way, we obtain a global map of the 5-year mean vertical column density of NO_2 in long-range transport events.

This will include plumes measured on multiple days and lead to an appropriate representation of the routes of longer-lasting plumes.

We perform this analysis for four seasons to illustrate the local seasonality of the phenomenon. The results can be seen in Fig. 19.

The data confirm the existence of hotspots of NO_2 long-range transport events in the mid-latitudes and typical transport routes along which NO_2 plumes travel. Note, that our algorithm only detects events over the ocean and routes over continental areas cannot be detected. This rules out thunderstorms and other individual events of NO_2 emissions as the dominant origin of events identified as long-range transport in this study. They may still be present as false positives.

There is a strong seasonality in the data. Plumes are most dominant in local autumn and winter and can only rarely be seen in local summer. Due to observational limitations, especially the route of North American and European plumes towards the Arctic cannot be fully observed in the data. However, the data strongly suggest export of European and North American NO_2 to Greenland and onto the Arctic Ocean where it might alter tropospheric chemistry.

Long-range transport events are only observed in mid- to higher latitudes (starting roughly at $\pm 40^\circ$ N) where cyclones are frequent along the storm tracks and the lifetime of NO_2 is sufficiently long to allow transport over multiple days. We detect no significant long-range transport events in the tropics.

While China exports NO_2 quite frequently, not much of it is seen crossing a significant portion of the Pacific. Most of the plumes appear to be entering Russia after a brief journey over the ocean. This circular motion is typical for plumes in the Northern Hemisphere – North America and Europe show it to a lesser extent – and can be attributed to the cyclones transporting the plume.

We identify the sources of NO_2 long-range transport events by creating a similar map (Fig. 20). Here, we project the NO_2 load of each pixel onto its origin, as determined by the last point in its backtrajectory. This produces a rough map of the relative source strength for NO_2 emitted into plumes of long-range transport events by that particular region.

We identify the following hot-spots: East Coast of North America, Central Europe, China, South Africa. Besides that, some plumes are also emitted from Argentina and Australia which only play a minor role. Europe is the only region which exhibits westward travel of plumes over the ocean.

It is not clear if all plumes in South Africa originate from the Highveld plateau or if individual observed plumes also originate from bush fires on the West Coast. These would only be a weak contribution to the overall signal which will be dominated by the strongly emitting Highveld industrial region and power plants. A large fraction of backtrajectories end on the coast East of the plateau. This is most likely due to the elevated emissions and descending wind following the geography from the plateau down to the ocean.

Even though we use only verified long-range transports, the emission data are highly scattered. This is due to the chaotic deviations resulting from long backtrajectories in strong wind shear. The coarse resolution necessary for this study amplifies this effect. Keeping this in mind, it is surprising, how sharply the emitters of long-range transports observed over the ocean are localized.

Investigations into the sources for plumes at different observed ages show that sources for plumes in their first day are sharply defined and the determined sources become more scattered with each day of plume age.

Fig. 21 shows an analogous map to Fig. 19, but here the NO_2 vertical column densities in long-range transport plumes are averaged over all seasons and instead binned by their respective plume age to show the temporal evolution of the routes. As expected, we find plumes with older ages at observation time at a larger distance from the emission regions and spread out more broadly than the young plumes. Also, the large number of plumes in the Baltic and North Sea, enclosed by emission regions (see Sect. 5.4), is apparent.

6.3 Regions

There are four major regions emitting NO_2 long-range transport events on the globe: the North American East Coast, Central Europe, South Africa and China. We have analyzed the plumes from these regions in further detail to gain more insight into the atmospheric conditions during long-range transport events and to quantify their impact on the global NO_2 distribution. The regions are highlighted in Fig. 22.

For each region, we only select plumes that moved from a continental area in the emission region out to the ocean in the observation region within the last 24 hours. This way, we make sure that no plumes are counted twice and we only select plumes that actually originate in the selected hot-spot region.

The frequency of long-range transport events differs strongly from region to region. North America and Europe emit a plume every 10 days on annual average, which corresponds to one plume every 5 days during winter. In contrast to that, South Africa emits plumes only every 17 days, while China emits one plume a week. This illustrates that NO_2 long-range transport is not a rare phenomenon and has been hidden from systematic scientific scrutiny only by cloud-filtering of satellite data.

6.3.1 Boundary NO_2 flux

First, we analyze the boundary flux of these regions. We sum up the NO_2 content of all the plumes in the respective region and normalize by the number of days of observation. This yields the total yearly export of NO_2 from the continent onto the ocean.

The data in Fig. 23 show, that the strongest emitter of plumes is China, followed by Europe. However, the plumes

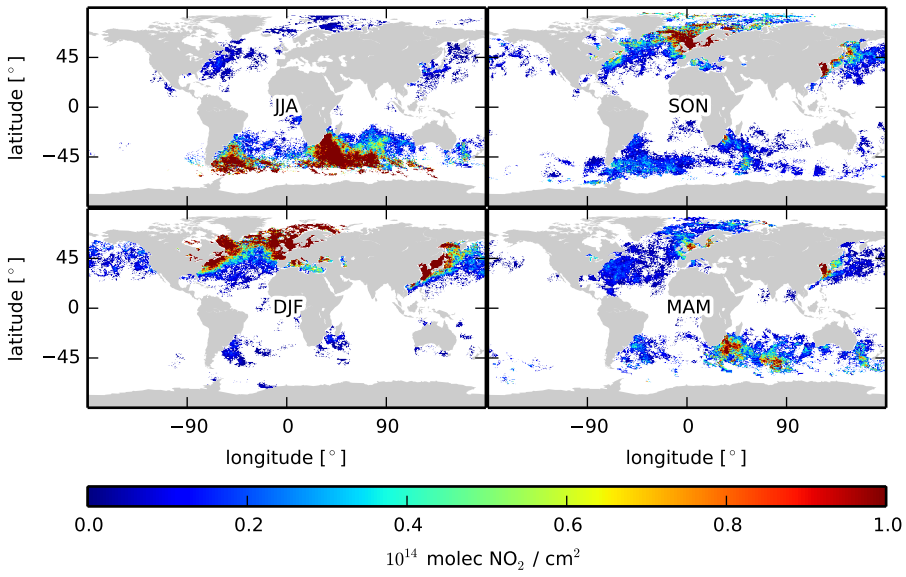

Fig. 19. Seasonal maps of the mean vertical column density of NO_2 observed in plumes associated to long-range transport events. Note that columns near Europe are always higher than columns near North America – at least partially due to its special geography.

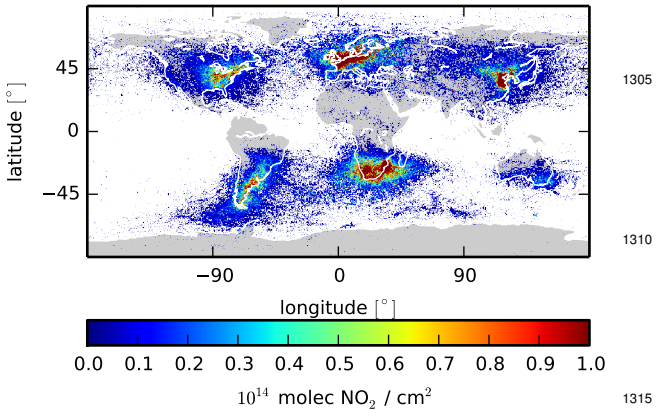

Fig. 20. Regional contribution to average NO_2 vertical column densities observed in long-range transport plumes. Sources of most long-range transport events are clearly visible. The high scatter originates from the low resolution of meteorological data used for the backtrajectories and uncertainties in the determination of the most likely backtrajectory.

from China do not last as long and do not form such a prominent route. It appears that South Africa experiences the opposing effect: here, plumes follow a very stable and visible route over the open ocean. This leads to small absolute emissions being strongly represented in the dataset.

The total outflux of these four regions amounts to more than $50\,\mathrm{GgN/a}$ in long-range transport events, which are exported to the ocean and remote regions. This is slightly more than a permil of the estimated global yearly NO_2 emission rate of $43\,\mathrm{TgN/a}$. This might appear to be a small fraction, but it constitutes a significant amount for such an unstable gas – especially, as our backtracing algorithm does not take the decay of NO_2 from emission to observation of the plume into account.

We also look at the regional differences in plume sizes. Fig. 24 shows that China and especially Europe emit a relatively large fraction of NO_2-rich long-range transport plumes. North America and South Africa tend to produce much smaller plumes.

6.3.2 Composite analysis of meteorological conditions

Finally, we take a look into large-scale meteorological conditions which accompany long-range transport events, using NCEP DOE AMIP-II Reanalysis data. We use a composite analysis which has been used in similar studies to analyze polar lows in the nordic seas (Blechschmidt et al., 2009) and NO_x transport in South Africa (Abiodun et al., 2014).

For each long-range transport event that we find in the given region, we collect meteorological conditions for various temporal offsets: two days before the plume has been emitted (according to backtrajectories) until the date of observation. For each offset we iterate over all retrieved long-range transport events and collect the meteorological conditions at the respective offset from emission (we call this the

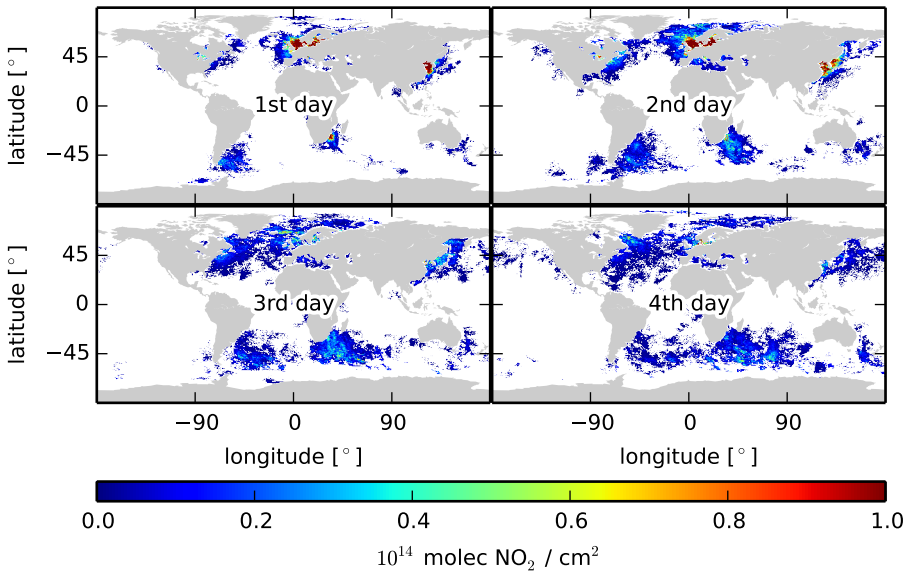

Fig. 21. Map of the mean NO_2 vertical column density observed in plumes of long-range transport events, binned by the age of plumes since emission at observation time.

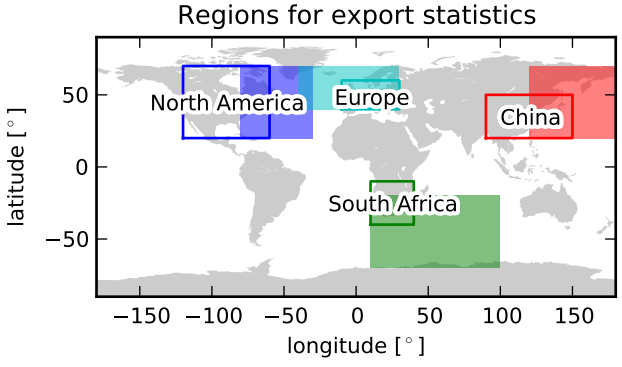

Fig. 22. The regions used for the statistical study. Only plumes are considered that were observed over the ocean in the filled rectangle and were found over land-masses in the open rectangle 24 hours earlier.

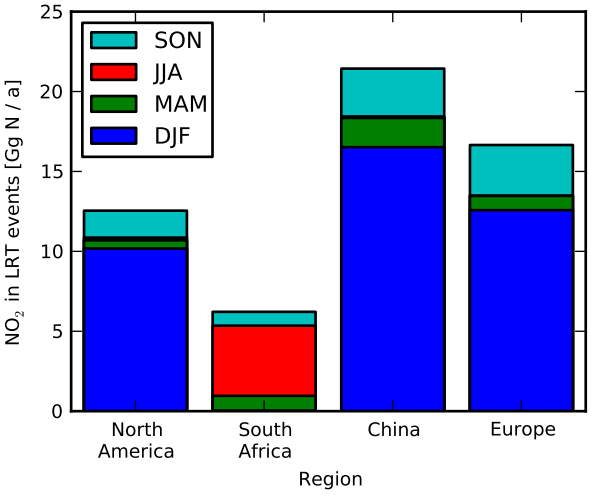

Fig. 23. Total yearly NO_2 content in long-range transport plumes emitted in the regions shown in Fig. 22 for different seasons.

related composite). All remaining observations are collected in the unrelated composite. This allows an analysis of the temporal evolution of the conditions and yields insight into the dominant meteorological conditions behind long-range transport events.

We allow for multiple observations of the same plume to enter the dataset as these stronger and more reliable events are a better indication of favorable conditions.

We restrict the analysis to the respective winter seasons: December, January and February (DJF) in the Northern Hemisphere; June, July and August (JJA) in the Southern Hemisphere. These are the months with the highest long-range transport event frequency and thus most suited to investigate the associated meteorological conditions.

Now, for various meteorological quantities, we have two disjoint sets of observations (or composites): observations related and unrelated to plume emission. The unrelated com-

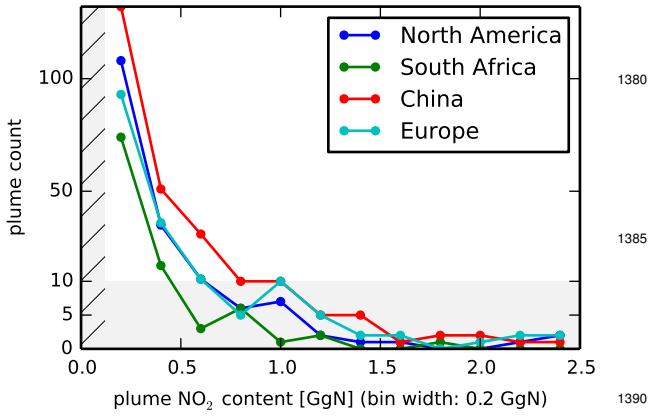

Fig. 24. NO_2 content distribution of long-range transport events observed in the respective regions. South Africa has the smallest plumes, while Europe emits a large fraction of NO_2-rich plumes. The data are binned in steps of $0.2\,GgN$. The hatched area denotes the NO_2 content below which plumes are not included in the analysis. The shaded area indicates a stretched axis to illustrate the frequency of plumes with high NO_2 content.

posite represents the climatological mean in the absence of NO_2 long-range transport events. We calculate the deviation of the average of both the related and the unrelated composite. Also, we use the Mann-Whitney U test (Mann and Whitney, 1947) to find significant deviations in the two distributions.

We perform this test for the mean sea level pressure, geopotential height at $500\,hPa$, surface air temperature, both our custom cloud product and the FRESCO+ cloud fraction and the NO_2 vertical column density. For the composite analysis, we did not interpolate values from NCEP DOE AMIP-II Reanalysis and GOME-2 and instead selected the nearest time step in the respective data set. This may lead to temporal discrepancies of up to 12 hours between the two data sets as we evaluate GOME-2 data only once a day.

Note, that the results from this analysis only show anomalies in the mean of these quantities. Movement of the anomaly over time does not have to result from a movement or other type of temporal evolution of signals in the meteorological input data. They could be merely a coincidence or result from a superposition of multiple patterns in the input data. However, a dominance of a single pattern in the input data will lead to this pattern appearing in the composite data.

One of the most prominent emitters, North America, does not shown any regular pattern that would yield insights into the process that leady to the emission of long-range transport events. There are not even systematically elevated NO_2 vertical column densities which are typical of long-range transport events. Most likely, this lack of systematics is due to a relatively broad region of high NO_2 emissions. When meteorological data from plumes from varying origin are superimposed, this will lead to diminishing systematics, leading to little or no significant signal.

In South Africa, we find that in the days leading up to and following the emission of a long-range transport plume, there is a pattern of alternating high- and low-pressure anomalies moving towards the East (Fig. 25). A low-pressure anomaly approaches South Africa and crosses the southern tip of the African continent one day after plume emission. Over the course of plume emission, this anomaly increases in strength. This anomaly indicates that, typically, passing low-pressure systems – or cyclones – lead to the emission of an NO_2 plume. As on the Southern Hemisphere cyclones rotate clockwise, this indicates that NO_2 plumes would typically be ejected from South Africa on a south-eastwards trajectory. This is confirmed in the statistical analysis.

Composites of GOME-2 observations show elevated NO_2 vertical column densities over the Highveld plateau, moving to the South-East over the lifetime of a long-range transport event (Fig. 26). After the plume is emitted, NO_2 vertical column densities show an anomaly towards lower values in the Highveld region, which indicates that NO_2 has actually been relocated. Strong fluctuations in NO_2 vertical column density are visible near polar night, where only few observations enter the data and GOME-2 observations show higher uncertainties.

In Europe (Fig. 27), the situation is similar. In the days preceeding a long-range transport event there is a strong anomaly towards reduced mean sea-level pressure over Western Europe of the order $\Delta P \approx -5\,hPa$. Contrasting this low-pressure anomaly, there is a high-pressure anomaly over the Arctic and Western Russia. These two anomalies form a channel which denotes the typical route observed in long-range transport events in this study. There is a low surface temperature anomaly over Europe and northern Russia during the days of transport, of order $\Delta T \approx -1 \ldots -3K$.

Eckhardt et al. (2003) have shown in simulations that the North Atlantic Oscillation (NAO) may be responsible for transport of pollutants to the Arctic, modeling trace gases with lifetimes of 5 days. Christoudias et al. (2012) find similar patterns of pollution export as shown in Fig. 19 to stem from zonal wind flow, resulting from the NAO. The results in Fig. 27 indicate a possible negative correlation to the NAO, with emissions of plumes being linked to a negative NAO index – showing a high-pressure anomaly over Iceland and a low-pressure anomaly over the Azores. The high-pressure anomaly over Iceland is, however, spatially extended, making these results ambiguous.

A correlation of plume frequency with monthly NAO indices from the NCEP Climate Prediction Center (http://www.cpc.ncep.noaa.gov/products/precip/CWlink/) over all months (Fig. 28) shows no significant correlation (probability of a random distribution generating such data: $32\,\%$). However, these two quantities exhibit two features: an uncorrelated part when few plumes are emitted and a highly

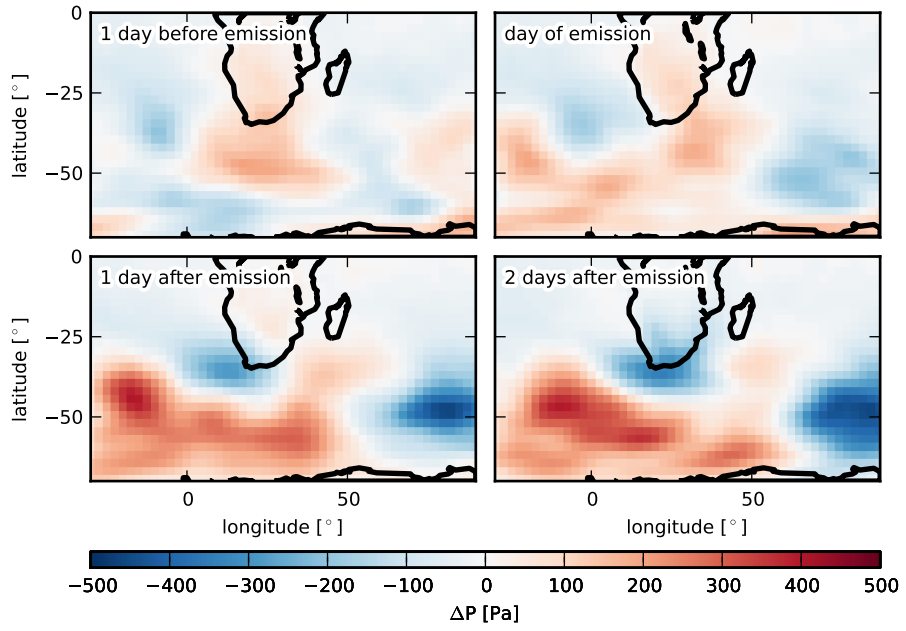

Fig. 25. NCEP DOE AMIP-II Reanalysis mean sea-level pressure anomaly (given in Pa) for the days of plume emission in the South African region. Only events in JJA (2007–2011) are shown, to prevent biases from meteorologic seasonality. The image shows significant high and low pressure patterns in the southern midlatitudes, moving from West to East.

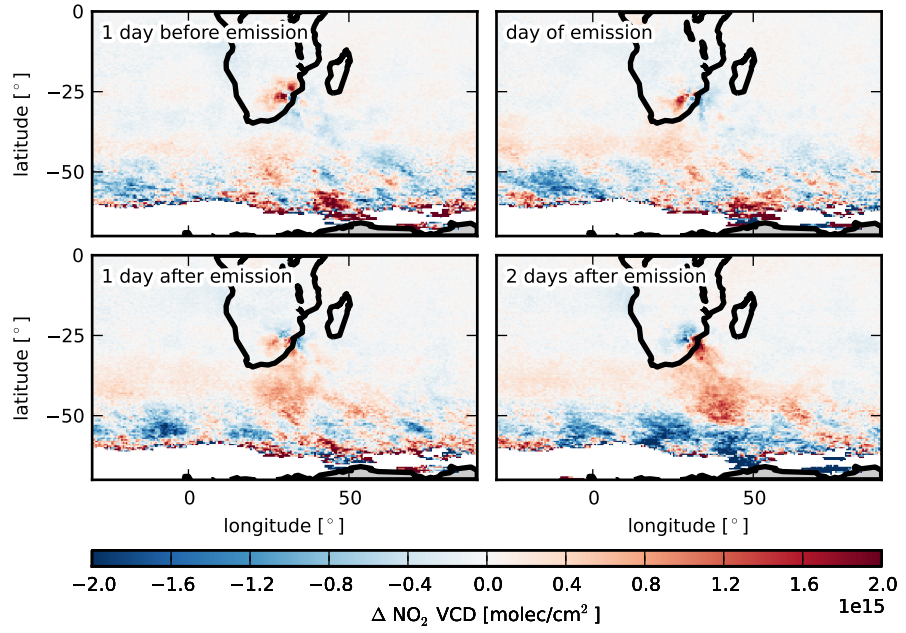

Fig. 26. GOME-2 tropospheric NO_2 vertical column density for the days of plume emission in the South African region. Only events in JJA (2007–2011) are shown, to prevent biases from meteorologic seasonality. There is an anomaly towards high values over the Highveld region before plume emission. After emission, the NO_2 vertical column densities over the Highveld region are on average lower, while an upwards anomaly can be seen southeast of South Africa. High fluctuations in the GOME-2 data and few observations result in visible noise in the anomalies near polar night.

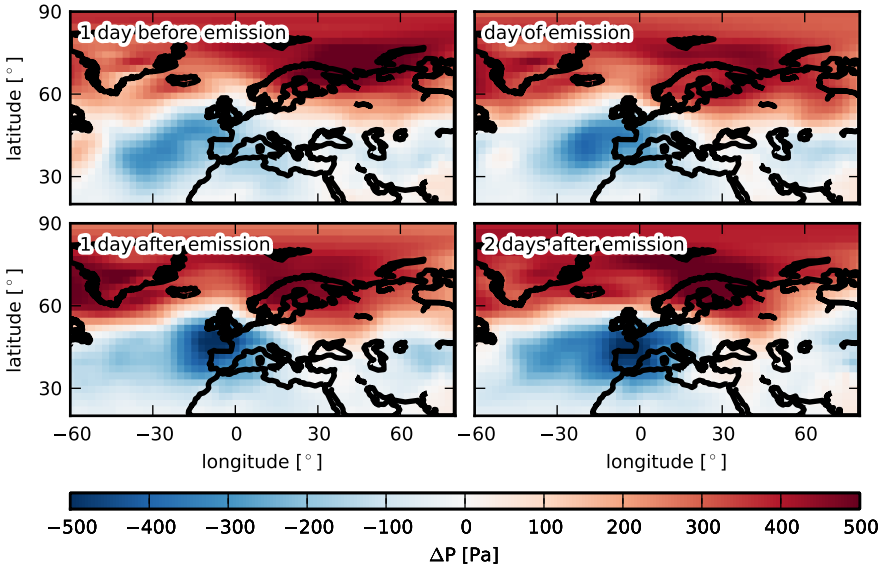

Fig. 27. As in Fig. 25, but for the Central European region. Only events in DJF (2007–2011) are shown. The data show a low-pressure anomaly over Western Europe over the course of the transport. Contrasting this, there is a high-pressure anomaly over the Arctic and Northern Russia.

correlated part when multiple plumes are emitted. When we remove all points with less than 5 plumes in the given month, the probability of a random distribution leading to these results is only $0.05\,\%$, making this result highly significant. Plume emission rated significantly increase with a lower NAO index. This confirms results from the composite analysis. Negative NAO indices with low plume frequency are almost entirely spring to late summer, which are unfavorable for NO_2 long-range transport due to radiation budget.

For long-range transport events originating from Europe, again, we find significantly elevated NO_2 vertical column densities over Europe, the North Sea and the North East Atlantic during the course of emission (Fig. 29).

Lastly, in China we find a strong upwards anomaly of NO_2 vertical column densities in the Beijing area in the days preceeding the emission of a long-range transport event. This anomaly only partly moves and dissolves after the emission. Long-range transport events are more likely to be observed when there are elevated NO_2 levels in the source regions. There is also a low-pressure anomaly over the Okhotsk Sea and the Kamchatka peninsula which is shifted to northern China over the course of the transport. This anomaly does not stay as concentrated after the emission and spreads over East Asia (Fig. 30).

These findings suggest that passing low-pressure systems or cyclones may be the dominant process leading to NO_2 long-range transport events in mid-latitudes. Elevated NO_2 concentrations in source regions are linked to the detection of these events.

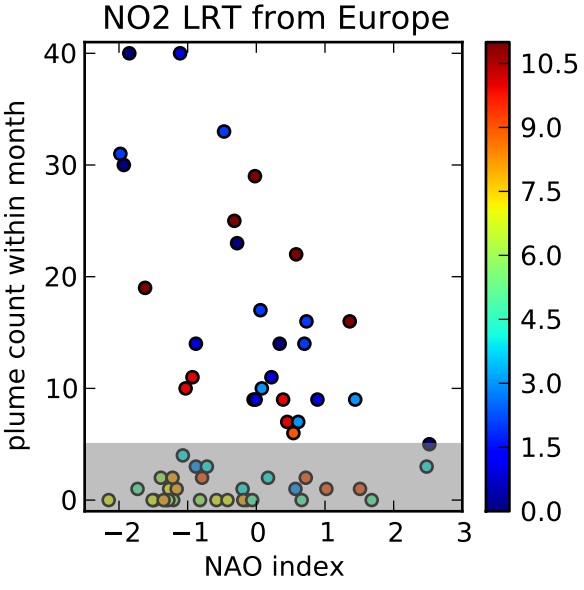

Fig. 28. Correlation of plume frequency in a given month with the NAO index as determined by the NCEP Climate Prediction Center. Colors denote the calendaric month (with 0 being December). Values in the shaded area were not considered for the correlation analysis. There are two superimposed features: no correlation during spring to late summer and a strong negative correlation during autumn and winter.

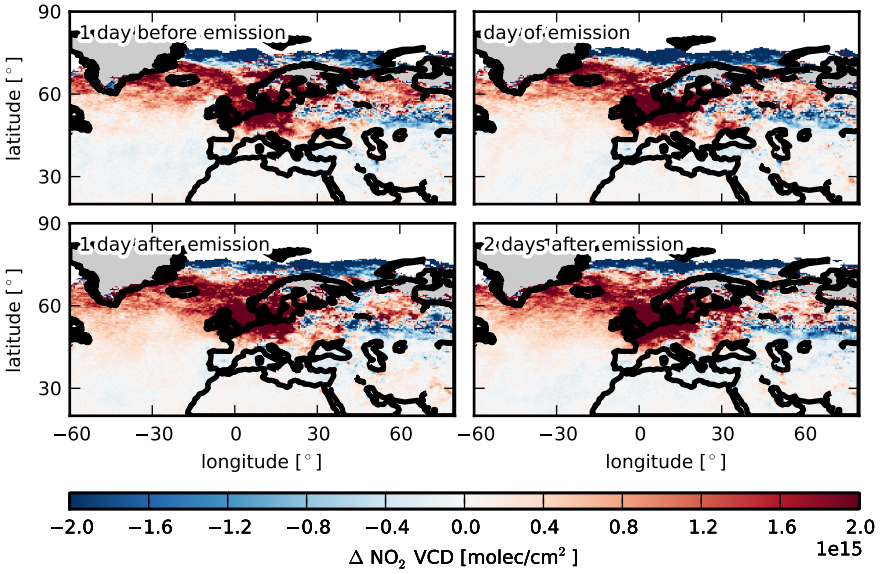

Fig. 29. As in Fig. 26, but for Europe and the North Sea. Only events in DJF (2007–2011) are shown. The data show significantly elevated levels of NO_2 vertical column density over Europe and the North Sea in the days before and during a long-range transport event.

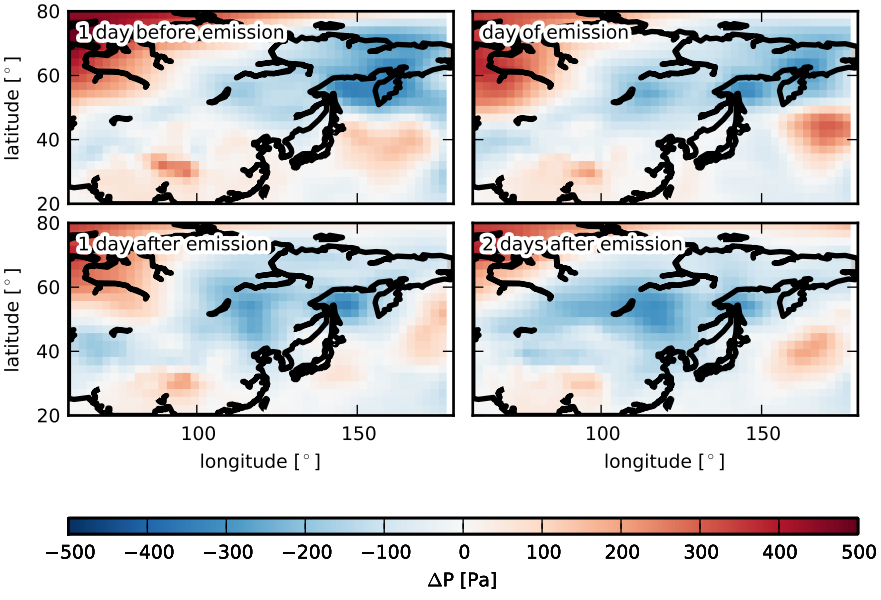

Fig. 30. As in Fig. 25, but for China and the Pacific. Only events in DJF (2007–2011) are shown. The data show a low-pressure anomaly moving from Russia towards northern China during the days preceeding and following plume emission.

7 Conclusions

We analyzed NO_2 long-range transport events globally using GOME-2 satellite data. For this, we had to take observations with cloudy scenes into account. We employed a simple approximation to determine the NO_2 vertical column density under cloudy conditions for an elevated plume.

We developed an algorithm that automatically identifies long-range transport events in these data. It detects short-lived positive anomalies of NO_2 vertical column densities

over the ocean and performs lagrangian backtracking to verify the anthropogenic origin of the event and to assess further plume properties. We then analyzed the resulting dataset of 3808 long-range transport events in GOME-2 data from 2007 to 2011.

We cannot distinguish NO_2 from anthropogenic sources and $LiNO_x$. However, their high frequency, distinguished seasonal and geographic distribution and the visibility of the observed events indicate that the majority of events found in the satellite data is not caused by thunderstorms, as $LiNO_x$ is rarely visible in observations of DOAS satellite instruments.

We found that NO_2 long-range transport events are a common phenomenon. There are four major hot-spots which emit NO_2 plumes subject to long-range transport: the North American East Coast, South Africa, China and Europe.

The NO_2 plumes travel along characteristic routes, leading to the polar circle for South Africa and into the Arctic for North America and Europe. The total amount of NO_2 transported in these events is surprisingly large considering the short lifetime in the boundary layer, where most emissions take place. Reservoir species of NO_2 are not detected and their likely presence will lead to an underestimation of the potential NO_2 impact on downwind regions. The actual impact on atmospheric chemistry of downwind regions will depend on the abundance of O_3, OH and NO_2, among others. Unfortunately, GOME-2 satellite data do not permit an analysis of transport events and their impact in the Arctic, which is likely to be one of the most sensitive regions to the effects of altered atmospheric and oceanic chemistry due to NO_2 long-range transports.

The emission shows strong seasonality, both in number and size of the plumes. More and larger plumes are emitted in winter, when the lifetime of NO_2 is long, anthropogenic emission rates are especially high and meteorological conditions are favorable with frequent cold fronts and cyclones. No long-range transport events have been identified in the tropics.

The meteorology responsible for these events appears to depend on the region. In North America, plumes follow storm tracks over the Atlantic, but show no distinct meteorological anomaly in a composite analysis. In Europe, long-range transports towards the Arctic appear to be linked to NAO phases. South Africa shows a typical pattern of alternating high and low pressure systems moving eastwards linked to plume emission.

It is likely that many events are triggered by a cyclone passing the emission region, accompanied by a cold front which lifts the NO_2 upwards into the free troposphere. There, wind speeds tend to be higher and the lifetime of NO_2 increases to the order of days, which is consistent with simple estimates from our analysis. Plumes can keep their distinct boundaries over days before they dilute.

Besides events from anthropogenic sources, we also observe events from Australia which appear to be caused by bushfires in the south of the continent. In at least one case, there is evidence that lightning occurred during an long-range transport event and might have added NO_2 to the plume, most likely leading to an overestimation of the life time and transport of anthropogenic NO_2.

NO_2 long-range transport events can transport air pollution from South Africa to Australia, from China to Japan and Taiwan and they are likely to have an impact on remote, pristine regions such as the Arctic.

Acknowledgements. This work is part of the INTAS project, funded by the Deutsche Forschungsgemeinschaft (DFG) and Universität Bremen. It was inspired by work of Andreas Heckel, see http://www.doas-bremen.de/posters/egu_2005_heckel.pdf. GOME-2 radiances have been provided by EUMETSAT. NCEP Reanalysis data provided by the NOAA/OAR/ESRL PSD, Boulder, Colorado, USA, from their web site at http://www.esrl.noaa.gov/psd/. NCEP EDAS and GDAS (FNL) Model Data (DSI-6141) provided by the NOAA/NCDC, Asheville, NC, USA, from their web site at http://www.ncdc.noaa.gov. The HYSPLIT model was provided by the NOAA/ARL. The authors wish to thank the World Wide Lightning Location Network (http://wwlln.net), a collaboration among over 50 universities and institutions, for providing the lightning location data used in this paper. We gratefully acknowledge Stefan Schreier's advice on biomass burning in Australia.

References

Abiodun, B. J., Ojumu, A. M., Jenner, S., and Ojumu, T. V.: The transport of atmospheric NOx and HNO3 over Cape Town, Atmos. Chem. Phys., 14, 559–575, doi:10.5194/acp-14-559-2014, http://www.atmos-chem-phys.net/14/559/2014/, 2014.

Aschmann, J., Sinnhuber, B.-M., Atlas, E. L., and Schauffler, S. M.: Modeling the transport of very short-lived substances into the tropical upper troposphere and lower stratosphere, Atmos. Chem. Phys., 9, 9237–9247, doi:10.5194/acp-9-9237-2009, http://www.atmos-chem-phys.net/9/9237/2009/, 2009.

Beirle, S., Platt, U., Wenig, M., and Wagner, T.: NOx production by lightning estimated with GOME, Advances in Space Research, 34, 793–797, doi:10.1016/j.asr.2003.07.069, http://www.sciencedirect.com/science/article/pii/S0273117704003576, 2004.

Beirle, S., Salzmann, M., Lawrence, M. G., and Wagner, T.: Sensitivity of satellite observations for freshly produced lightning NOx, Atmos. Chem. Phys., 9, 1077–1094, doi:10.5194/acp-9-1077-2009, http://www.atmos-chem-phys.net/9/1077/2009/, 00000, 2009.

Beirle, S., Boersma, K. F., Platt, U., Lawrence, M. G., and Wagner, T.: Megacity Emissions and Lifetimes of Nitrogen Oxides Probed from Space, Science, 333, 1737–1739, doi:10.1126/science.1207824, http://www.sciencemag.org/content/333/6050/1737, 2011.

Blechschmidt, A.-M., Bakan, S., and Graßl, H.: Large-scale atmospheric circulation patterns during polar low events over the Nordic seas, Journal of Geophysical Research: Atmospheres, 114, n/a–n/a, doi:10.1029/2008JD010865, http://onlinelibrary.wiley.com/doi/10.1029/2008JD010865/abstract, 2009.

Boersma, K. F., Eskes, H. J., and Brinksma, E. J.: Error analysis for tropospheric NO2 retrieval from space, Journal of Geophysical Research: Atmospheres, 109, n/a–n/a, doi:10.1029/2003JD003962, http://onlinelibrary.wiley.com/doi/10.1029/2003JD003962/abstract, 2004.

Bovensmann, H., Burrows, J. P., Buchwitz, M., Frerick, J., Noël, S., Rozanov, V. V., Chance, K. V., and Goede, A. P. H.: SCIAMACHY: Mission Objectives and Measurement Modes, Journal of the Atmospheric Sciences, 56, 127–150, doi:10.1175/1520-0469(1999)056<0127:SMOAMM>2.0.CO;2, http://journals.ametsoc.org/doi/abs/10.1175/1520-0469(1999)056%3C0127:SMOAMM%3E2.0.CO;2, 1999.

Burrows, J., Hölzle, E., Goede, A., Visser, H., and Fricke, W.: SCIAMACHY—scanning imaging absorption spectrometer for atmospheric chartography, Acta Astronautica, 35, 445–451, doi:10.1016/0094-5765(94)00278-T, http://www.sciencedirect.com/science/article/pii/009457659400278T, 1995.

Burrows, J. P., Weber, M., Buchwitz, M., Rozanov, V., Ladstätter-Weißenmayer, A., Richter, A., DeBeek, R., Hoogen, R., Bramstedt, K., Eichmann, K.-U., Eisinger, M., and Perner, D.: The Global Ozone Monitoring Experiment (GOME): Mission Concept and First Scientific Results, Journal of the Atmospheric Sciences, 56, 151–175, doi:10.1175/1520-0469(1999)056<0151:TGOMEG>2.0.CO;2, http://journals.ametsoc.org/doi/abs/10.1175/1520-0469(1999)056%3C0151:TGOMEG%3E2.0.CO%3B2, 1999.

Callies, J., Corpaccioli, E., Eisinger, M., Hahne, A., and Lefebvre, A.: GOME-2 - Metop's Second Generation sensor for Operational Ozone Monitoring, ESA Bulletin, 102, 2000.

Christian, H. J.: Optical Detection of Lightning from Space, in: Proceedings of the 11th International Conference on Atmospheric Electricity, 715-718, Guntersville, Alabama, http://thunder.nsstc.nasa.gov/lis/, 1999.

Christian, H. J., R. J. Blakeslee, S. J. Goodman, D. A. Mach, M. F. Stewart, D. E. Buechler, W. J. Koshak, J. M. Hall, W. L. Boeck, K. T. Driscoll, and D. J. Bocippio: The Lightning Imaging Sensor, in: Proceedings of the 11th International Conference on Atmospheric Electricity, pp. 746–749, Guntersville, Alabama, http://thunder.nsstc.nasa.gov/bookshelf/pubs/LIS_ICAE99_Print.pdf, 1999.

Christoudias, T., Pozzer, A., and Lelieveld, J.: Influence of the North Atlantic Oscillation on air pollution transport, Atmos. Chem. Phys., 12, 869–877, doi:10.5194/acp-12-869-2012, http://www.atmos-chem-phys.net/12/869/2012/, 2012.

Crawford, J., Olson, J., Davis, D., Chen, G., Barrick, J., Shetter, R., Lefer, B., Jordan, C., Anderson, B., Clarke, A., Sachse, G., Blake, D., Singh, H., Sandolm, S., Tan, D., Kondo, Y., Avery, M., Flocke, F., Eisele, F., Mauldin, L., Zondlo, M., Brune, W., Harder, H., Martinez, M., Talbot, R., Bandy, A., and Thornton, D.: Clouds and trace gas distributions during TRACE-P, Journal of Geophysical Research, 108, 13 PP., doi:200310.1029/2002JD003177, http://www.agu.org/pubs/crossref/2003/2002JD003177.shtml, 2003.

Dentener, F., Keating, T., and Akimoto, H.: Hemispheric transport of air pollution, Tech. rep., United Nations, Geneva, http://htap.org/publications/2010_report/2010_Final_Report/HTAP%202010%20Part%20A%20110407.pdf, 2010.

Draxler, R.: HYSPLIT4 user's guide, 1999.

Draxler, R. and Hess, G.: Description of the HYSPLIT_4 modeling system, NOAA Tech. Memo. ERL ARL-224, NOAA Air Resources Laboratory, Silver Spring, MD, 1997.

Draxler, R. and Hess, G.: An overview of the HYSPLIT_4 modeling system of trajectories, dispersion, and deposition, Aust. Meteor. Mag., 47, 295–308, 1998.

Eckhardt, S., Stohl, A., Beirle, S., Spichtinger, N., James, P., Forster, C., Junker, C., Wagner, T., Platt, U., and Jennings, S. G.: The North Atlantic Oscillation controls air pollution transport to the Arctic, Atmospheric Chemistry and Physics, 3, 1769–1778, http://www.atmos-chem-phys.net/3/1769/2003/acp-3-1769-2003.pdf, 2003.

Ehhalt, D. H., Rohrer, F., and Wahner, A.: Sources and Distribution of NO$_x$ in the Upper Troposphere at Northern Mid-Latitudes, Journal of Geophysical Research, 97, PAGES 3725–3738, http://www.agu.org/journals/jd/v097/iD04/91JD03081/, 1992.

Franke, K., Richter, A., Bovensmann, H., Eyring, V., Jöckel, P., Hoor, P., and Burrows, J. P.: Ship emitted NO2 in the Indian Ocean: comparison of model results with satellite data, Atmospheric Chemistry and Physics, 9, 7289–7301, doi:10.5194/acp-9-7289-2009, http://www.atmos-chem-phys.org/9/7289/2009/acp-9-7289-2009.html, 2009.

Giles, D. M., Holben, B. N., Eck, T. F., Sinyuk, A., Smirnov, A., Slutsker, I., Dickerson, R. R., Thompson, A. M., and Schafer, J. S.: An analysis of AERONET aerosol absorption properties and classifications representative of aerosol source regions, Journal of Geophysical Research: Atmospheres, 117, n/a–n/a, doi:10.1029/2012JD018127, http://onlinelibrary.wiley.com/doi/10.1029/2012JD018127/abstract, 2012.

Hilboll, A., Richter, A., and Burrows, J. P.: Long-term changes of tropospheric NO2 over megacities derived from multiple satellite instruments, Atmos. Chem. Phys., 13, 4145–4169, doi:10.5194/acp-13-4145-2013, http://www.atmos-chem-phys.net/13/4145/2013/, 2013.

Hild, L., Richter, A., Rozanov, V., and Burrows, J. P.: Air mass factor calculations for GOME measurements of lightning-produced NO2, Advances in Space Research, 29, 1685–1690, doi:10.1016/S0273-1177(02)80014-X, http://www.sciencedirect.com/science/article/B6V3S-46K7X59-5Y/2/5ba0393000f7be137b8e5ade96eac62e, 2002.

Horowitz, L. W., Walters, S., Mauzerall, D. L., Emmons, L. K., Rasch, P. J., Granier, C., Tie, X., Lamarque, J.-F., Schultz, M. G., Tyndall, G. S., Orlando, J. J., and Brasseur, G. P.: A global simulation of tropospheric ozone and related tracers: Description and evaluation of MOZART, version 2, Journal of Geophysical Research (Atmospheres), 108, 4784, doi:10.1029/2002JD002853, http://adsabs.harvard.edu/abs/2003JGRD..108.4784H, 2003.

Inness, A., Baier, F., Benedetti, A., Bouarar, I., Chabrillat, S., Clark, H., Clerbaux, C., Coheur, P., Engelen, R. J., Errera, Q., Flemming, J., George, M., Granier, C., Hadji-Lazaro, J., Huijnen, V., Hurtmans, D., Jones, L., Kaiser, J. W., Kapsomenakis, J., Lefever, K., Leitão, J., Razinger, M., Richter, A., Schultz, M. G., Simmons, A. J., Suttie, M., Stein, O., Thépaut, J.-N., Thouret, V., Vrekoussis, M., Zerefos, C., and the MACC team: The MACC reanalysis: an 8 yr data set of atmospheric composition, Atmos. Chem. Phys., 13, 4073–4109, doi:10.5194/acp-13-4073-2013, http://www.atmos-chem-phys.net/13/4073/2013/, 2013.

Kalnay et al.: The NCEP/NCAR 40-year reanalysis project, Bull. Amer. Meteor. Soc., 77, 437–470, 1996.

Kokhanovsky, A. and Rozanov, V.: Retrieval of NO2 vertical columns under cloudy conditions: A sensitivity study based on SCIATRAN calculations, Atmospheric Research, 93, 695–699, doi:10.1016/j.atmosres.2009.01.022, http://www.sciencedirect.com/science/article/B6V95-4VS400C-3/2/00d2efcb75f755abf250785c5f1354fb, 2009.

Labonne, M., Bréon, F.-M., and Chevallier, F.: Injection height of biomass burning aerosols as seen from a spaceborne lidar, Geophysical Research Letters, 34, n/a–n/a, doi:10.1029/2007GL029311, http://onlinelibrary.wiley.com/doi/10.1029/2007GL029311/abstract, 2007.

Leitão, J., Richter, A., Vrekoussis, M., Kokhanovsky, A., Zhang, Q. J., Beekmann, M., and Burrows, J. P.: On the improvement of NO2 satellite retrievals – aerosol impact on the airmass factors, Atmospheric Measurement Techniques, 3, 475–493, doi:10.5194/amt-3-475-2010, http://www.atmos-meas-tech.net/3/475/2010/amt-3-475-2010.html, 2010.

Leue, C., Wenig, M., Wagner, T., Klimm, O., Platt, U., and Jähne, B.: Quantitative analysis of NO x emissions from Global Ozone Monitoring Experiment satellite image sequences, Journal of Geophysical Research: Atmospheres, 106, 5493–5505, doi:10.1029/2000JD900572, http://onlinelibrary.wiley.com/doi/10.1029/2000JD900572/abstract, 2001.

Lin, M., Holloway, T., Carmichael, G. R., and Fiore, A. M.: Quantifying pollution inflow and outflow over East Asia in spring with regional and global models, Atmos. Chem. Phys., 10, 4221–4239, http://www.atmos-chem-phys.net/10/4221/2010/, 2010.

Mann, H. B. and Whitney, D. R.: On a Test of Whether one of Two Random Variables is Stochastically Larger than the Other, The Annals of Mathematical Statistics, 18, 50–60, doi:10.1214/aoms/1177730491, http://projecteuclid.org/euclid.aoms/1177730491, 1947.

Martin, R. V., Chance, K., Jacob, D. J., Kurosu, T. P., Spurr, R. J. D., Bucsela, E., Gleason, J. F., Palmer, P. I., Bey, I., Fiore, A. M., Li, Q., Yantosca, R. M., and Koelemeijer, R. B. A.: An improved retrieval of tropospheric nitrogen dioxide from GOME, Journal of Geophysical Research (Atmospheres), 107, 4437, http://adsabs.harvard.edu/abs/2002JGRD..107.4437M, 2002.

Martin, R. V., Jacob, D. J., Chance, K., Kurosu, T. P., Palmer, P. I., and Evans, M. J.: Global inventory of nitrogen oxide emissions constrained by space-based observations of NO2 columns, Journal of Geophysical Research: Atmospheres, 108, n/a–n/a, doi:10.1029/2003JD003453, http://onlinelibrary.wiley.com/doi/10.1029/2003JD003453/abstract, 2003.

National Climatic Data Center, NESDIS, NOAA, U.S. Department of Commerce: NCEP EDAS and GDAS (FNL) Model Data (DSI-6141), http://www.ncdc.noaa.gov.

Ott, L. E., Pickering, K. E., Stenchikov, G. L., Allen, D. J., DeCaria, A. J., Ridley, B., Lin, R.-F., Lang, S., and Tao, W.-K.: Production of lightning NOx and its vertical distribution calculated from three-dimensional cloud-scale chemical transport model simulations, Journal of Geophysical Research: Atmospheres, 115, n/a–n/a, doi:10.1029/2009JD011880, http://onlinelibrary.wiley.com/doi/10.1029/2009JD011880/abstract, 2010.

Palmer, P. I., Jacob, D. J., Chance, K., Martin, R. V., Spurr, R. J. D., Kurosu, T. P., Bey, I., Yantosca, R., Fiore, A., and Li, Q.: Air mass factor formulation for spectroscopic measurements from satellites: Application to formaldehyde retrievals from the Global Ozone Monitoring Experiment, Journal of Geophysical Research: Atmospheres, 106, 14 539–14 550, doi:10.1029/2000JD900772, http://onlinelibrary.wiley.com/doi/10.1029/2000JD900772/abstract, 2001.

Platt, U. and Stutz, J.: Differential Optical Absorption Spectroscopy: Principles and Applications, Springer, Berlin, 1 edn., 2007.

Popp, C., Wang, P., Brunner, D., Stammes, P., Zhou, Y., and Grzegorski, M.: MERIS albedo climatology for FRESCO+ O$_2$ A-band cloud retrieval, Atmospheric Measurement Techniques, 4, 463–483, doi:10.5194/amt-4-463-2011, http://www.atmos-meas-tech.net/4/463/2011/amt-4-463-2011.html, 2011.

Rastigejev, Y., Park, R., Brenner, M. P., and Jacob, D. J.: Resolving intercontinental pollution plumes in global models of atmospheric transport, http://www.agu.org/pubs/crossref/2010/2009JD012568.shtml, 2010.

Richter, A. and Burrows, J. P.: Tropospheric NO2 from GOME measurements, Advances in Space Research, 29, 1673–1683, doi:10.1016/S0273-1177(02)00100-X, http://www.sciencedirect.com/science/article/B6V3S-46K7X59-5X/2/11216e36f5a64e7a3a3e9ee6f7385134, 2002.

Richter, A., Burrows, J. P., N|[uuml]||[szlig]|, H., Granier, C., and Niemeier, U.: Increase in tropospheric nitrogen dioxide over China observed from space, Nature, 437, 129–132, doi:10.1038/nature04092, http://www.nature.com/nature/journal/v437/n7055/full/nature04092.html, 2005.

Richter, A., Begoin, M., Hilboll, A., and Burrows, J. P.: An improved NO$_2$ retrieval for the GOME-2 satellite instrument, Atmospheric Measurement Techniques, 4, 1147–1159, doi:10.5194/amt-4-1147-2011, http://www.atmos-meas-tech.net/4/1147/2011/amt-4-1147-2011.html, 2011.

Riuttanen, L., Dal Maso, M., de Leeuw, G., Riipinen, I., Sogacheva, L., Vakkari, V., Laakso, L., and Kulmala, M.: Long-range transport of biomass burning smoke to Finland in 2006, Atmospheric Chemistry and Physics Discussions, 13, 4289–4330, doi:10.5194/acpd-13-4289-2013, http://www.atmos-chem-phys-discuss.net/13/4289/2013/acpd-13-4289-2013.html, 2013.

Rozanov, A., Rozanov, V., Buchwitz, M., Kokhanovsky, A., and Burrows, J.: SCIATRAN 2.0 – A new radiative transfer model for geophysical applications in the 175-2400 nm spectral region, Advances in Space Research, 36, 1015–1019, doi:10.1016/j.asr.2005.03.012, http://www.sciencedirect.com/science/article/pii/S0273117705002887, 2005.

Rozanov, V., Rozanov, A., Kokhanovsky, A., and Burrows, J.: Radiative transfer through terrestrial atmosphere and ocean: Software package SCIATRAN, Journal of Quantitative Spectroscopy and Radiative Transfer, doi:10.1016/j.jqsrt.2013.07.004, http://www.sciencedirect.com/science/article/pii/S0022407313002872.

Sauvage, B., Cammas, J., Defer, E., Volz-Thomas, A., Thomas, K., and Holle, R. L.: Lightning NOx influence on large scale NOy and O3 plumes observed over the northern mid-latitudes, AGU Fall Meeting Abstracts, -1, 0187, http://adsabs.harvard.edu/abs/2011AGUFM.A51A0187S, 2011.

Schaub, D., Weiss, A. K., Kaiser, J. W., Petritoli, A., Richter, A., Buchmann, B., and Burrows, J. P.: A transboundary transport episode of nitrogen dioxide as observed from GOME and its impact in the Alpine region, Atmos. Chem. Phys., 5, 23–37, doi:10.5194/acp-5-23-2005, http://www.atmos-chem-phys.

net/5/23/2005/, 2005.

Schultz, M., Schmitt, R., Thomas, K., and Volz-Thomas, A.: Photochemical box modeling of long-range transport from North America to Tenerife during the North Atlantic Regional Experiment (NARE) 1993, Journal of Geophysical Research, 103, 13 477–13,488, doi:10.1029/97JD01481, http://www.agu.org/pubs/crossref/1998/97JD01481.shtml, 1998.

Schumann, U. and Huntrieser, H.: The global lightning-induced nitrogen oxides source, Atmos. Chem. Phys., 7, 3823–3907, doi:10.5194/acp-7-3823-2007, http://www.atmos-chem-phys.net/7/3823/2007/, 2007.

Singh, H. B. and Hanst, P. L.: Peroxyacetyl nitrate (PAN) in the unpolluted atmosphere: An important reservoir for nitrogen oxides, Geophysical Research Letters, 8, 941–944, doi:10.1029/GL008i008p00941, http://onlinelibrary.wiley.com/doi/10.1029/GL008i008p00941/abstract, 1981.

Sodemann, H., Pommier, M., Arnold, S. R., Monks, S. A., Stebel, K., Burkhart, J. F., Hair, J. W., Diskin, G. S., Clerbaux, C., Coheur, P.-F., Hurtmans, D., Schlager, H., Blechschmidt, A.-M., Kristjánsson, J. E., and Stohl, A.: Episodes of cross-polar transport in the Arctic troposphere during July 2008 as seen from models, satellite, and aircraft observations, Atmos. Chem. Phys., 11, 3631–3651, doi:10.5194/acp-11-3631-2011, http://www.atmos-chem-phys.net/11/3631/2011/, 00009, 2011.

Solomon, S., Schmeltekopf, A. L., and Sanders, R. W.: On the interpretation of zenith sky absorption measurements, Journal of Geophysical Research, 92, 8311–8319, http://adsabs.harvard.edu/abs/1987JGR....92.8311S, 1987.

Spichtinger, N., Wenig, M., James, P., Wagner, T., Platt, U., and Stohl, A.: Satellite detection of a continental-scale plume of nitrogen oxides from boreal forest fires, Geophysical Research Letters, 28, 4579–4582, http://www.agu.org/pubs/crossref/2001/2001GL013484.shtml, 2001.

Stohl, A., Huntrieser, H., Richter, A., Beirle, S., Cooper, O. R., Eckhardt, S., Forster, C., James, P., Spichtinger, N., and Wenig, M.: Rapid intercontinental air pollution transport associated with a meteorological bomb, Atmos. Chem. Phys., 3, 969–985, http://www.atmos-chem-phys.net/3/969/2003/acp-3-969-2003.pdf, 2003.

Stohl, A., Forster, C., Frank, A., Seibert, P., and Wotawa, G.: Technical note: The Lagrangian particle dispersion model FLEXPART version 6.2, Atmos. Chem. Phys., 5, 2461–2474, doi:10.5194/acp-5-2461-2005, http://www.atmos-chem-phys.net/5/2461/2005/, 00523, 2005.

van der A, R. J., Eskes, H. J., Boersma, K. F., van Noije, T. P. C., Van Roozendael, M., De Smedt, I., Peters, D. H. M. U., and Meijer, E. W.: Trends, seasonal variability and dominant NOx source derived from a ten year record of NO2 measured from space, Journal of Geophysical Research: Atmospheres, 113, n/a–n/a, doi:10.1029/2007JD009021, http://onlinelibrary.wiley.com/doi/10.1029/2007JD009021/abstract, 2008.

Vrekoussis, M., Wittrock, F., Richter, A., and Burrows, J. P.: Temporal and spatial variability of glyoxal as observed from space, Atmos. Chem. Phys., 9, 4485–4504, doi:10.5194/acp-9-4485-2009, http://www.atmos-chem-phys.net/9/4485/2009/, 2009.

Walker, T. W., Martin, R. V., van Donkelaar, A., Leaitch, W. R., MacDonald, A. M., Anlauf, K. G., Cohen, R. C., Bertram, T. H., Huey, L. G., Avery, M. A., Weinheimer, A. J., Flocke, F. M., Tarasick, D. W., Thompson, A. M., Streets, D. G., and Liu, X.: Trans-Pacific transport of reactive nitrogen and ozone to Canada during spring, Atmos. Chem. Phys., 10, 8353–8372, doi:10.5194/acp-10-8353-2010, http://www.atmos-chem-phys.net/10/8353/2010/, 2010.

Wang, P., Stammes, P., van der A, R., Pinardi, G., and van Roozendael, M.: FRESCO+: an improved O2 A-band cloud retrieval algorithm for tropospheric trace gas retrievals, Atmos. Chem. Phys., 8, 6565–6576, doi:10.5194/acp-8-6565-2008, http://www.atmos-chem-phys.net/8/6565/2008/, 2008.

Wenig, M., Spichtinger, N., Stohl, A., Held, G., Beirle, S., Wagner, T., Jähne, B., and Platt, U.: Intercontinental transport of nitrogen oxide pollution plumes, Atmospheric Chemistry and Physics, 3, 387–393, http://hal.archives-ouvertes.fr/hal-00295247, 2003.

Whittaker, L. M. and Horn, L. H.: Northern Hemisphere extratropical cyclone activity for four mid-season months, Journal of Climatology, 4, 297–310, doi:10.1002/joc.3370040307, http://onlinelibrary.wiley.com/doi/10.1002/joc.3370040307/abstract, 1984.

Wittrock, F., Richter, A., Oetjen, H., Burrows, J. P., Kanakidou, M., Myriokefalitakis, S., Volkamer, R., Beirle, S., Platt, U., and Wagner, T.: Simultaneous global observations of glyoxal and formaldehyde from space, Geophysical Research Letters, 33, L16 804, doi:10.1029/2006GL026310, http://onlinelibrary.wiley.com/doi/10.1029/2006GL026310/abstract, 2006.